UNIVERSITY OF CALIFORNIA
RIVERSIDE

Enhanced Properties in Thermally Stable Ultrafine Grained and Nanocrystalline Silver Alloys Through Severe Plastic Deformation Processing

A Dissertation submitted in partial satisfaction
of the requirements for the degree of

Doctor of Philosophy

in

Materials Science and Engineering

by

Erik William Sease

December 2021

Dissertation Committee:

Dr. Suveen N. Mathaudhu, Chairperson
Dr. Peter A. Greaney
Dr. Boniface P. T. Fokwa

The Dissertation of Erik William Sease is approved:

_____

_____

_____

Committee Chairperson

University of California, Riverside

Acknowledgements

I would firstly like to acknowledge and thank my advisor Dr. Suveen Mathaudhu for being an excellent advisor and supporting me during my entire grad school career, and for pushing me to pursue a PhD in the first place – I would not have made it this far without his help. I would also like to thank Dr. Alex Greaney, Dr. Boniface Fokwa, Dr. Jun Sheng and Dr. Kandis Leslie Abdul-Aziz for serving on my qualifying exam and defense committees and for providing much appreciated advice and critique on my work. Secondly, I would like to thank everyone in my research group, as well as other students, researchers and faculty at UC Riverside who helped me learn everything that has allowed me to make it to this point. Lastly, I would like to thank all the other friends, dogs, family and everyone else who has made this a fun and exciting journey and supported me along the way.

Un-Acknowledgements

I would *not* like to thank the COVID-19 pandemic for putting kind of a damper on my last two years of grad school. That was a bummer for sure.

ABSTRACT OF THE DISSERTATION

Mechanical and Electrical Properties in Thermally Stable Ultrafine Grained and Nanocrystalline Silver Alloys Through Severe Plastic Deformation Processing

by

Erik William Sease

Doctor of Philosophy, Graduate Program in Materials Science and Engineering
University of California, Riverside, December 2021
Dr Suveen N. Mathaudhu, Chairperson

Metallic silver has been extensively used by humans for millennia, with usage recorded as far back as 4000 BCE due to its abundance of useful material properties including corrosion resistance and high formability, making it an ideal metal for use by ancient civilizations. In more recent centuries other properties such as the oligodynamic effect, which gives rise to antimicrobial properties in silver, as well as the highest thermal and electrical conductivity of any metal, have helped silver retain the interest of scholars and scientists in numerous disciplines. Several issues with silver however have reduced its use in many applications in which it would otherwise be an ideal material choice. Some material properties of silver, in particular the mechanical strength and extremely low stacking fault energy, make silver a very poor choice for structural purposes, which require a high resistance to deformation. Pure silver possesses very low hardness and strength and has a tendency to gall under repeated loading and unloading. While it is possible to strengthen silver through a variety of strengthening mechanisms, including work hardening or reduction of the grain size (i.e., Hall-Petch strengthening), the low stacking fault energy of silver makes it energetically favorable for dislocations to dissociate into partial

dislocations with a wide equilibrium splitting distance. While this tendency of dislocations to dissociate allows silver to obtain extremely high dislocation densities, it acts as a driving force for recovery, recrystallization and grain growth within the crystal lattice. The poor mechanical properties and low stacking fault energy in silver culminate in a material which self-anneals at room temperature, losing the increased strength and hardness imparted by materials processing techniques used to strengthen it.

In this work, we explore two severe plastic deformation methods for strengthening of silver – mechanical alloying combined with spark plasma sintering, and high pressure torsion. Microstructural stabilization through dilute alloying additions and impurities is explored for prevention of self-annealing, producing ultrafine grained and nanocrystalline high strength silver and silver alloys with high thermal stability and resistance to grain growth.

TABLE OF CONTENTS

List of Figures

List of Tables

CHAPTER 1: INTRODUCTION

1.1 Overview

Severe plastic deformation (SPD) processing techniques are a family of materials processing techniques commonly used for strengthening of metals. These processes use the application of immense pressure to impart high levels of plastic strain to materials without causing significant change in the net geometric shape of the material [1]. By constraining a material within a die to prevent free flow while introducing high amounts of strain into the lattice of a metal, extremely high dislocation densities can be generated within a polycrystalline material. As dislocations are introduced to the strained metal, they form low angle grain boundaries, which, as they continue to absorb more dislocations, eventually decompose into a highly refined grain structure, separated by high angle grain boundaries [2]. This reduction of the grain size in a polycrystalline material to the sub-micron or even the nanometer scale is a well-studied strengthening mechanism known as Hall-Petch strengthening, also commonly referred to as grain boundary strengthening [3]. The term nanocrystalline (NC) is used to refer to polycrystalline materials with a grain size under 100nm, and ultrafine-grained (UFG) is used to define grain sizes between 100-1000nm [4]. By reducing the grain size of these materials to the nanoscale, the mechanical properties of materials processed by SPD are drastically increased, allowing production of metals with strength or hardness orders of magnitude greater than generally observed in coarse grained metals, or materials not processed by SPD.

SPD processes are analogous to commonly used metals processing techniques such as extrusion, forging, rolling, and countless others which can strengthen a material through grain structure refinement [5]. One significant distinction between these more common used processing techniques and SPD techniques is the confinement of the material in a die, which increases the amount of strain that can be imparted to the material during processing. While common processes

may only apply a plastic strain of up to about 2.0 [6], SPD processing techniques may introduce a plastic strain multiple orders of magnitude higher than this [6], which, as well as refining the grain size, introduces vastly increased dislocation density in the material which further acts to increase the mechanical properties [7].

1.2 Motivation

The vastly superior mechanical properties displayed by NC and UFG materials introduces increased potential for structural purposes in comparison to their coarse-grained counterparts, especially in metals not commonly considered to be structural materials. Structural materials are, as the name suggests, materials which are used primarily for their mechanical properties, such as strength, hardness, toughness, or elasticity, as opposed to other materials properties such as electrical, magnetic, optical, etc. By applying SPD processes to materials not generally known for their mechanical properties, we can expand their use into novel structural applications.

Silver is one such metal which has fallen out of use as a structural metal. Silver is one of the oldest metals used by humans due to its high formability and resistance to corrosion, with use as coinage material, water vessels and tools dating back at least 6,000 years [8]. Despite its use as such in the past, silver is not traditionally considered a structural material in modern circumstances, as it is relatively soft and deforms easily in comparison to modern structural metals such as steel or aluminum alloys [9].

As well as its poor mechanical properties, silver also possesses an extremely low stacking fault energy (SFE) of $16 mJ/m^2$ [10] in comparison to other pure metals, such as $45 mJ/m^2$ in copper [10] or $220 mJ/m^2$ in aluminum [11]. Dislocations present within a low SFE metal lattice will tend to dissociate into two partial dislocations to reduce elastic energy, with larger equilibrium separation distances corresponding to lower SFE [12]. This large splitting distance

hinders dislocation climb and cross-slip and dislocation annihilation, creating forests of pinned sessile dislocations and much higher dislocation densities than observed in lower SFE metals [12,13]. While this high dislocation density leads to increased mechanical properties compared to the non-work hardened or annealed state, it also acts as a driving force for recovery and grain growth, leading to exceptionally poor thermal stability, yielding self-annealing and recrystallization at room temperature and loss of hardness within days of processing [10]. These particularly poor mechanical properties of silver often overshadow some of its more useful properties, such as the highest thermal and electrical conductivity of any pure metal, and highly effective antimicrobial properties, despite low toxicity to humans [8, 14-16].

In order to make use of silver's useful material properties within a broader range of structural applications, it becomes necessary to: 1) Improve its mechanical properties, and 2) Increase the thermal stability of silver to prevent self-annealing and softening. One of the most basic methods of increasing the mechanical strength of a pure metal is by alloying with other elements. Through the addition of one or more alloying elements to the metal lattice metal, solid solution strengthening and introduction of additional phases increase the strength of the lattice metal by introducing stresses and barriers in the lattice which impede the motion of dislocations through the metal. Alloying and additional phases however yield a significant reduction in the electrical conductivity [16] which reduces its attractiveness of silver or other highly conductive materials in applications which require high electrical conductivity. By reducing the alloying additions in a silver alloy to a minimum and strengthening through other mechanisms, it becomes possible to avoid some of the detrimental effects of alloying or second phases [17] on silver's exceptional conductivity.

1.3 Objectives

The following sections of this dissertation detail the processing-properties-performance-structure relationship of dilute high strength nanocrystalline silver alloys processed by two different severe plastic deformation processing techniques to explore the feasibility and applications of metallic silver in non-traditional applications. By exploring the development of techniques for producing enhanced mechanical properties in this material system, we may gain insight into the possibility for application of these methods in other materials systems and their use in non-traditional applications.

The primary objectives of this dissertation are as follows:

1) Develop an understanding of the fundamental interactions between processing, structure, properties, and performance in high strength silver alloys processed through severe plastic deformation (SPD) processing methods.

2) Understanding of the strengthening mechanisms present in SPD processed high strength silver alloys, the individual contributions to mechanical properties offered by each, and the limitations of each, as well as the effect of processing on non-mechanical properties of these alloys.

3) Understanding of the effect of time and temperature on the long-term thermal stability and self-annealing behavior on the mechanical properties in silver alloys processed through SPD processes.

These objectives should be considered in how they apply to SPD processing for the alloys explored in this work, as well as their use and context in the processing of metallic materials in general. By developing an understanding of the use of SPD processing on the properties non-traditional structural materials, we may develop a deeper understanding and gain insights into the

potential use and effect of SPD processing on the properties in other non-traditional structural alloy systems.

1.4 Processing Techniques

In order to explore the strengthening and microstructural stabilization of silver alloys through SPD processing, two commonly used SPD processes were selected based on their availability at the time of this research and for their ability to produce exceptionally high levels of grain refinement in polycrystalline materials, strengthening them without the need for alloying additions or second phase particles through the aforementioned Hall-Petch relationship. Although they are not strictly necessary, the addition of dilute alloying additions and impurities are explored in this work in order to determine their effects on strengthening and microstructural stabilization.

The Hall-Petch relationship is the observed and empirically demonstrated relationship between the yield strength and grain size of a polycrystalline metal, alloy, or intermetallic [3, 18]:

$$\sigma_Y = \sigma_0 + kd^{-\frac{1}{2}} \quad (1)$$

Where σ_Y is the yield strength of the material at a given grain size d, σ_0 is the lattice friction stress, or the stress required to move a dislocation within a perfect crystalline lattice of the material, and k is the strengthening coefficient; a material dependent constant which measures the local stress needed to initiate plastic flow within the material. Grain boundaries in metallic materials act as barriers to dislocation motion due to lattice misorientation and mismatch, preventing slip and deformation. As the volume fraction of grain boundaries within the material increases, the amount of applied stress necessary to overcome the critical stress needed to move dislocations between grains increases, generating an increase in the yield strength of the material. The two SPD processes used to explore the fabrication of microstructurally stable high strength bulk silver alloys are as follows: mechanical alloying combined with consolidation by spark

plasma sintering, and high pressure torsion. These two processes approach SPD from two separate directions, and each has inherent advantages over the other process: Mechanical alloying is considered a ”bottom-up” method, while HPT is considered a “top-down” processing method; the distinction being that in bottom-up processes, bulk nanostructured material is produced through assembly of small nanoparticles or nanostructured solids, while top-down processes begin with a bulk scale coarse-grained material and refines the existing coarse microstructure through processing [1].

1.4.1 Mechanical Alloying and Spark Plasma Sintering

1.4.1.1 Mechanical Alloying

The first SPD process, explored further in Chapter 2, is mechanical alloying (MA), also know ass mechanical milling, ball milling, mechanical attrition, and a number of other names. Fundamentally, MA consists of repeated fracturing, cold welding, and re-fracturing of metal powder particles through repeated abrasion or collisions with hardened metal or ceramic milling media in the form of balls or rods, all within a closed container. MA is classified as an SPD process, as the milling introduces high levels of strain within the microstructure of powder particles, yielding grain refinement within the individual particles through an increase in dislocation density [19]. Repeated collisions between the milling media and powder particles causes a flattening and work hardening of the particles as they are deformed by repeated collisions.

As these particles are further fractured and flattened, they begin to overlap and bring clean metal surfaces into contact, which then become cold welded as collisions continue. As dislocation density within the material increases, dislocations eventually form low angle boundaries as they align, annihilate, and recombine. Sub-grain and low angle grain boundaries eventually absorb more dislocations, and accompanied by grain rotation, decompose into smaller

grains, separated by high angle grain boundaries [20]. Eventually the competing mechanisms of fracturing and cold welding create a highly refined and homogenized microstructure as the grain size of the material approaches a material-specific minimum, independent of milling conditions [20].

The minimum grain size for FCC metals such as silver has been found to scale inversely with the melting temperature T_m or bulk modulus B of the material, i.e. the higher the T_m or B, the smaller the minimum grain size [21]. This is believed to be due to competition between work hardening and recovery phenomena of the metals (such as activation energy for self-diffusion), which scale with the melting point.

As the refined material produced by MA is in powder form, it is necessary to pair it with secondary consolidation processes to form bulk material and is therefore considered a bottom-up process. Most consolidation processes for metallic powders such as traditional sintering involve long hold times at elevated temperature, however this causes recrystallization in NC metals due to the high driving force for recovery caused by the large presence of grain boundaries within NC metals.

1.4.1.2 Spark Plasma Sintering

Spark plasma sintering (SPS), also known as pulsed electric current sintering (PECS), field assisted sintering technique (FAST), and a variety of other names, is a relatively new powder consolidation process, combining aspects of sintering and hot pressing. Despite its similarities to traditional sintering, the mechanism for heating is Joule heating (resistive heating) of the work material itself, which provides numerous advantages over traditional sintering or pressing, which use external heating sources [22, 23]. Despite the name, there is now a general consensus that the process does not produce plasma [24, 25].

Consolidation by SPS utilizes a combination of uniaxial pressure and pulsed DC current to consolidate powders in an electrically conductive die. A mechanical loading system applies pressure to a punch and die assembly, inside which a bed of powder is confined. A high current upwards of several thousand amps [37] is applied across the punch and die assembly at low voltage, generating internal heating within the powder bed. The punch and die assembly are held within a vacuum chamber which protects the tooling and powder from atmospheric contamination and oxidation at elevated temperatures. The combination of pressure and current gives rise to enhanced sintering behavior compared to other consolidation processes [26], producing bulk disc-shaped samples which can easily be scaled up with larger SPS units.

Among the benefits of SPS are its extremely fast heating rate and its effect on the final microstructure of the powder bed. While traditional sintering processes may provide heating rates on the order of tens of degrees Celsius per minute, it is not uncommon for Joule heating in SPS to produce heating rates upwards of 1000°C per minute in some cases [26]. By applying a high heating rate to the powder bed, it is possible to quickly reach peak sintering temperature where densification and sintering between powder particles is most prominent.

Significantly shorter hold times are also common in SPS compared to standard sintering, with hold times often on the order of minutes, rather than hours [4]. By using the SPS process to consolidate NC powders produced through the MA process, the highly refined and plastically strained powder does not have the necessary time required to coarsen at elevated temperatures where grain boundary mobility is enhanced. The bulk material produced retains the mechanical properties inherent in the fine grain sizes due to the Hall-Petch effect [23]. Some coarsening is generally observed in samples processed by SPS; however, it is far less than that caused by traditional sintering.

1.4.2 High Pressure Torsion

High pressure torsion, commonly abbreviated as HPT, is an SPD process used to achieve grain refinement in a coarse-grained bulk precursor material and is therefore classified as a top-down SPD process. As the name suggests, HPT utilizes the application of immense pressure combined with torsion to refine the microstructure of a material: A disc shaped sample is placed between two anvils in a constrained die and subjected to a combination of applied uniaxial pressure on the order of several GPa, and torsional strain by twisting of the lower anvil [1]. As the lower anvil turns with respect to the top, frictional forces from the anvil deform the disc by shear and introduce a high dislocation density into the material, yielding grain refinement believed to occur through dynamic recovery, dynamic recrystallization and grain boundary migration due to the high density of accumulated lattice defects [27].

The strain introduced to the work material by HPT processing can be quantified by true strain, ε_{True}, where N is the number of revolutions of HPT, r is the radial distance, and h is the height of the disc [11]:

$$\varepsilon_{True} = ln(\frac{2\pi Nr}{h}) \quad (2)$$

Or by von Mises equivalent strain, which is more commonly seen in literature [11]:

$$\varepsilon_{Equivalent} = \frac{2\pi Nr}{h\sqrt{3}} \quad (3)$$

As there is a dependence on radial distance, the imposed plastic strain in the material should be at a maximum at the outer edge of the disc, and theoretically zero at the center of the disc. With enough revolutions however, prior studies [11, 28] have shown that with enough straining, both by higher pressure or more revolutions of HPT, a reasonable homogeneity across the disc can be reached as shear forces cause local hardening and transferal of shearing to adjacent positions within the disc [28].

One benefit of HPT processing is that the radial dependence of heterogeneity within the disc can be an effective tool for examining a wide range of applied strains within the material. The effect of time and imposed strain on the microstructural stability can be examined over a wide range of strains, indicating whether there are certain levels of plastic strain which may be prone to self-annealing, or a saturation point of dislocation density, past which recovery and recrystallization begin to occur. Other benefits to the HPT process are more inherent to top-down processing methods: HPT does not require the use of powders and milling media, which are far more prone to contamination than can introduce unpredictable microstructural evolution and mechanical properties [2]. Since HPT samples are not produced from powder precursor, it also avoids the issue of residual porosity which can have detrimental effects on the mechanical properties of materials processed by powder means. The applied pressure also prevents void formation and tearing of the sample during processing, producing high density material.
Top-down processing by HPT also comes with its own drawbacks however, including a difficulty in the scale-up of these processes. The limited depth of microstructural evolution caused by the torsion applied to samples restricts HPT to thin samples, on the order of millimeters in thickness. Other bulk SPD processes like MA and SPS on the other hand may produce considerably larger samples, with thicknesses on the order of centimeters.

1.5 Summary of Opportunity

The opportunities made possible by the work outlined in this dissertation align with the primary objectives laid out in section 1.3 of this chapter. Studies have been performed on SPD processing and strengthening of silver and silver alloys, and the poor thermal stability of SPD processed silver has been documented and explored through microstructural examination. By understanding the fundamental interaction between processing, structure, properties, and performance in high strength silver, this work seeks to elucidate processing methods for synthesis

of bulk high strength silver and dilute silver alloys with high thermal stability. The effect of strengthening by grain refinement and strain hardening on the electrical conductivity of these materials is also investigated for high strength high conductivity applications.

1.6 References

[1] Zhilyaev, A., & Langdon, T. (2008). *Using high-pressure torsion for metal processing: Fundamentals and applications*. Progress in Materials Science, 53(6), 893–979. doi:10.1016/j.pmatsci.2008.03.002

[2] Cordero, Z. C., Knight, B. E., & Schuh, C. A. (2016). *Six decades of the Hall–Petch effect – a survey of grain-size strengthening studies on pure metals. International Materials Reviews, 61(8), 495–512.* doi:10.1080/09506608.2016.1191808

[3] Hall, E. O. (1951). *The Deformation and Ageing of Mild Steel: III Discussion of Results*. Proceedings of the Physical Society. Section B, 64(9), 747–753. doi:10.1088/0370-1301/64/9/303

[4] Liu, D. et al, (2016). *Microstructure and mechanical behavior of NS/UFG aluminum prepared by cryomilling and spark plasma sintering*. Journal of Alloys and Compounds, 679, 426–435. doi:10.1016/j.jallcom.2016.04.073

[5] Valiev, R. et al, (2000). *Bulk nanostructured materials from severe plastic deformation*. Progress in Materials Science, 45(2), 103–189. doi:10.1016/s0079-6425(99)00007-9

[6] Azushima, A. et al. (2008). *Severe plastic deformation (SPD) processes for metals*. CIRP Annals, 57(2), 716–735. doi:10.1016/j.cirp.2008.09.005

[7] Hegedűs, Z. et al, (2012). *Microstructure of low stacking fault energy silver processed by different routes of severe plastic deformation*. Journal of Alloys and Compounds, 536, S190–S193. doi:10.1016/j.jallcom.2011.10.070

[8] Alexander, J. W. (2009). *History of the Medical Use of Silver*. Surgical Infections, 10(3), 289–292. doi:10.1089/sur.2008.9941

[9] S. Praiphruk, G. Lothongkum, E. Nisaratanaporn, and B. Lohwongwatana, "*Investigation of supersaturated silver alloys for high hardness jewelry application*", J. Met. Mater. Miner., vol. 23, no. 2, Dec. 2013.

[10] Matsunaga, H., & Horita, Z. (2009). *Softening and Microstructural Coarsening without Twin Formation in FCC Metals with Low Stacking Fault Energy after Processing by High-Pressure Torsion*. Materials Transactions, 50(7), 1633–1637. doi:10.2320/matertrans.mf200921

[11] Rohatgi, A., et al. *The influence of stacking fault energy on the mechanical behavior of Cu and Cu-Al alloys: Deformation twinning, work hardening, and dynamic recovery*. Metall Mater Trans A 32, 135–145 (2001). https://doi.org/10.1007/s11661-001-0109-7

[12] Qi, Y., & Mishra, R. K. (2007). *Ab initiostudy of the effect of solute atoms on the stacking fault energy in aluminum*. Physical Review B, 75(22). doi:10.1103/physrevb.75.224105

[13] Hegedűs, Z. et al, (2012). *Microstructure of low stacking fault energy silver processed by different routes of severe plastic deformation*. Journal of Alloys and Compounds, 536, S190–S193. doi:10.1016/j.jallcom.2011.10.070

[14] Mijnendonckx, K., Leys, N., Mahillon, J., Silver, S., & Van Houdt, R. (2013). *Antimicrobial silver: uses, toxicity and potential for resistance. BioMetals, 26(4), 609–621.* doi:10.1007/s10534-013-9645-z

[14] Praveen Kumar, S., Parameshwaran, R., Arun Kumar, S., Nathiya, S., & Heenalisha, K. (2020). *Electrical and mechanical studies on pure-silver coated aluminium based electrical contact materials. Materials Today: Proceedings.* doi:10.1016/j.matpr.2020.05.666

[15] Medici, S. et al, (2019). *The medical uses of silver: history, myths and scientific evidence*. Journal of Medicinal Chemistry. doi:10.1021/acs.jmedchem.8b01439

[16] Sakai, Y., et al, (1992). *Development of a high strength, high conductivity copper-silver alloy for pulsed magnets.* IEEE Transactions on Magnetics, 28(1), 888–891. doi:10.1109/20.120021

[17] Mineta, T., Saito, T., Yoshihara, T., & Sato, H. (2019). *Structure and mechanical properties of nanocrystalline silver prepared by spark plasma sintering.* Materials Science and Engineering: A, 754, 258–264. doi:10.1016/j.msea.2019.03.101

[18] Petch, N.J., (1953). *The cleavage strength of polycrystals*. J. of the Iron and Steel Inst. 174 25–28.

[19] J. Kozlik et al, *Cryogenic Milling of Titanium*, Metals 2018, 8, 31; doi:10.3390/met8010031

[20] M. H. Enayati & F. A. Mohamed (2014). *Application of mechanical alloying/ milling for synthesis of nanocrystalline and amorphous materials*. International Materials Reviews, 59:7, 394-416, DOI: 10.1179/1743280414Y.0000000036

[21] J. Eckert et al, (1992). *Investigation of Nanometer-Sized FCC Metals Prepared by Ball Milling*. Materials Science Forum, 88-90, 505–512, 1992. doi:10.4028/www.scientific.net/msf.88-90.505

[22] 25 Series, Fuji Electronic Industrial Co, Ltd., Spark Plasma Sintering Machine, Fuji-SPS. http://fuji-sps.sakura.ne.jp/products/25series/e_25series.html

[23] O. Guillon et al, (2014). *Field-Assisted Sintering Technology/Spark Plasma Sintering: Mechanisms*, Materials and Technology Developments, Advanced Engineering Materials, Vol. 16, Issue 7, 830-849. doi.org/10.1002/adem.201300409

[24] D. M. Hubert et al, *The absence of plasma in "spark plasma sintering"*, J. Appl. Phys. 104, 033305 (2008); https://doi.org/10.1063/1.2963701

[25] D. M. Hubert et al, (2009). *A discussion on the absence of plasma in spark plasma sintering*, Scripta Materialia 60, 835–83, doi: 10.1016/j.scriptamat.2008.12.059

[26] Z. A. Munir et al, (2006). *The effect of electric field and pressure on the synthesis and consolidation of materials: A review of the spark plasma sintering method*. J Mater Sci 41, 763-777, doi:10.1007/s10853-006-6555-2

[27] Edalati, K. et al, (2018). *Effect of temperature rise on microstructural evolution during high-pressure torsion.* Materials Science and Engineering: A, 714, 167–171. doi:10.1016/j.msea.2017.12.095

[28] Zhilyaev, A. et al, 2003). *Experimental parameters influencing grain refinement and microstructural evolution during high-pressure torsion.* Acta Materialia, 51(3), 753–765. doi:10.1016/s1359-6454(02)00466-4

Chapter 2: Strengthening Mechanisms in a Dilute Nanocrystalline Silver-Titanium Alloy Processed by Cryomilling and Spark Plasma Sintering

2.0 Abstract

Improvements in the mechanical strength of a dilute silver-titanium alloy are explored through a combination of powder processing and densification methods in order to produce bulk metallic samples, strengthened through multiple coexisting mechanisms. Strengthening is achieved through a collaboration between grain refinement, solid solutionizing, and dispersion strengthening achieved by mechanical alloying (MA) and spark plasma sintering (SPS) of silver powder with 1% titanium by weight. The strengthening mechanisms are characterized, and their relative contributions discussed and compared to previously published literature on silver, and through characterization of bulk samples by SEM, TEM, XRD and indentation. The results forecast processing-microstructure-property relationships needed for the manufacturing of high-strength nanocrystalline silver alloys.

2.1 Introduction

Silver is one of the oldest metals discovered by humans; found in native form and used for millennia for its numerous beneficial properties, including good formability and corrosion resistance, disinfectant properties, and the highest thermal and electrical conductivities of any pure metal [1-4]. Unfortunately, these benefits are often overshadowed by the poor mechanical properties of silver [5], preventing its use in most structural applications. Due to its high electrical conductivity, one of the most appealing applications of silver is in electrical connectors, but due to its low wear resistance and tendency to gall [6,7] under repeated loading and unloading, it is only used in low-durability and low-cycle applications [7]. In order to make use of silver's beneficial properties for a broader range of structural applications, it becomes necessary to bolster its mechanical properties such as strength and hardness.

One of the simplest methods of increasing the mechanical strength of a metal is by alloying with other elements. Alloying however yields a significant reduction in the electrical conductivity of silver [7] which reduces its attractiveness as an electrical conductor. In a study by Y. Sakai et al on the conductivity of Cu-Ag alloys, it was found that the addition of 2at% silver to a copper alloy reduced the conductivity by roughly 14-17% [8]. By keeping the alloying additions in a silver alloy to a minimum and strengthening by other means, we can avoid some of the detrimental effects of alloying on conductivity.

The reduction of the size of the grains or crystallites within the material, also known as grain boundary strengthening or Hall-Petch strengthening [9], is a well-studied method of increasing the mechanical properties of a metal, without the use of alloying additions or secondary phases. By reducing the grain size of structural materials to the nanoscale, it is possible to drastically increase their strength and hardness [9]. The superior mechanical properties displayed by nanocrystalline (NC) (<100 nm) and Ultrafine-Grained (UFG) (100 – 1000 nm) materials introduces a high level of potential for use as structural metals in comparison to their coarse-grained counterparts.

In this study, a bulk NC alloy of silver with 1% titanium by weight is produced via powder metallurgy through a combination of mechanical alloying (MA) performed at cryogenic temperatures (cryomilling) [10], and spark plasma sintering (SPS). The MA process is highly effective at dispersing alloying additions into the silver matrix, as well as grain refinement, as the milling media collides repeatedly with the powder during milling. The powder particles are repeatedly flattened, fractured, and cold welded back together, exposing clean surfaces and creating new grain boundaries [11]. By reducing the powder to cryogenic temperatures, the ductility of the silver is reduced, increasing the ratio of particle fracture versus particle welding by suppressing recovery and dynamic recrystallization [12]. Through this process, grain size in

the powder is effectively reduced to the nanometric scale through an increase in dislocation density and formation of grain boundaries as dislocations align, annihilate, and recombine [12]. Breakdown of the milling media during the MA process also introduces small amounts of second phase dispersoids into the silver matrix, further strengthening this alloy through the Orowan mechanism.

Through the combination of both the MA and SPS processing, this process yields a dilute silver alloy strengthened by grain refinement, solid solution strengthening, and dispersion strengthening, with a hardness over five times that of pure annealed silver [13] with near theoretical density.

2.2 Methods and Materials

2.2.1 Mechanical Alloying

Elemental silver powder (99.9% purity, -325 mesh particle size) and one percent titanium powder by weight (99.99% purity, -230 mesh particle size) purchased from Alfa Aesar was sealed in a 55mL tungsten carbide (WC) milling vial under argon atmosphere and subjected to MA in a modified high energy SPEX 8000D shaker mill. MA was performed with four 7/16” diameter tungsten carbide balls as milling media, with a ball to powder ratio of 10, and continuously milled for four hours. The mill design was modified by introducing a constant flow of liquid nitrogen between the tungsten carbide milling vial and a PTFE housing during milling, thereby lowering the temperature of the jar and powder to cryogenic temperatures while preventing direct contact between the powder and liquid nitrogen.

2.2.2 Powder Consolidation via Spark Plasma Sintering

Mechanically alloyed powders were removed from the vials under argon atmosphere, ground lightly with a mortar and pestle to break up agglomerates and sieved to isolate powders under 125 microns (-120 mesh particle size). Cylindrical graphite dies with a height of 30mm,

external diameter of 30mm and internal diameter of 10.3mm were loaded with 1g of milled and sieved Ag-1Ti powder. Cylindrical graphite punches of 10mm diameter were then inserted on either side hold the powder in place. The punch-and-die assembly was loaded into an SPS unit (Dr. Sinter Lab Jr. SPS-211LX) under a vacuum pressure of <3 Pa and compressed with a pre-load uniaxial ram pressure of 5 MPa. To study the effect of peak temperature on densification, temperature was ramped at a rate of 100°C per minute to peak temperatures between 350-700°C, measured with a K-type thermocouple inserted into a pocket on the side of the die. The 5 MPa pre-loading pressure was held until the thermocouple read peak temperature, which allowed for degassing of the powder and prevention of gas pocket entrapment in the final sintered material [14]. Once peak temperature was reached, the ram pressure was raised to 80 MPa to increase densification the powder bed. The powder was held at peak temperature for 5 minutes, after which the SPS was powered off. The die cooled in the SPS *in vacuo* under 80 MPa uniaxial ram pressure to 200°C before reducing ram pressure and removing the assembly from the SPS chamber. Through this method, bulk SPS discs of this Ag-1Ti silver alloy with a diameter of 10mm and thickness of 1mm were produced.

2.2.3 Microstructural and Mechanical Properties Characterization

The density of the sintered Ag-1Ti discs was measured with Archimedes' method in propylene glycol to determine their density relative to the theoretical density of bulk Ag-1Ti. X-ray diffraction scans were performed on the sintered discs in a PANalitycal Empyrean Series 2 XRD, and crystallite size was evaluated by Scherrer's equation using a full-width half maximum estimation of the Ag(111) peak. Sintered discs were cut in half radially and mounted in epoxy to expose their interior surfaces, which were then polished to a mirror finish with 0.05μm diamond suspension. The polished surfaces were subjected to indentation with a Phase II Vickers Micro Hardness Tester at a load of 200g and a dwell time of 15 seconds.

The microstructure was evaluated via SEM (ThermoFisher Scientific NNS450) to determine the underlying sources of strengthening. Focused ion beam (FIB) milling in a Duobeam Quanta 200i was used to extract a foil via FIB lift-out from the interior surface of the discs. These foils were examined in a TEM (ThermoFisher Scientific Tecnai12) to validate grain size measurements estimated using Scherrer's method. For comparison of hardness at larger grain sizes and determination of Hall-Petch coefficients, small buttons of the alloy were cast, mounted, and polished using the same methods mentioned before. Grain size was measured using the line intercept method and Vickers hardness indentation to give data for larger grain sizes.

2.3 Results

2.3.1 Peak SPS Temperature Relation to Density and Vickers Hardness

Figure 1 displays final sintered relative density and Vickers microhardness of this alloy as a function of peak sintering temperature for discs SPS processed at peak temperatures between 350 and 700°C. The density increases as a function of peak SPS temperature, with the largest growth in densification observed in samples between 350-600°C. Above 600°C densification slows and peaks at 98% relative density for samples SPS processed at 700°C. Vickers hardness increases up to 1.5 GPa in samples SPS processed at 550°C, followed by a reduction in hardness at higher SPS temperatures.

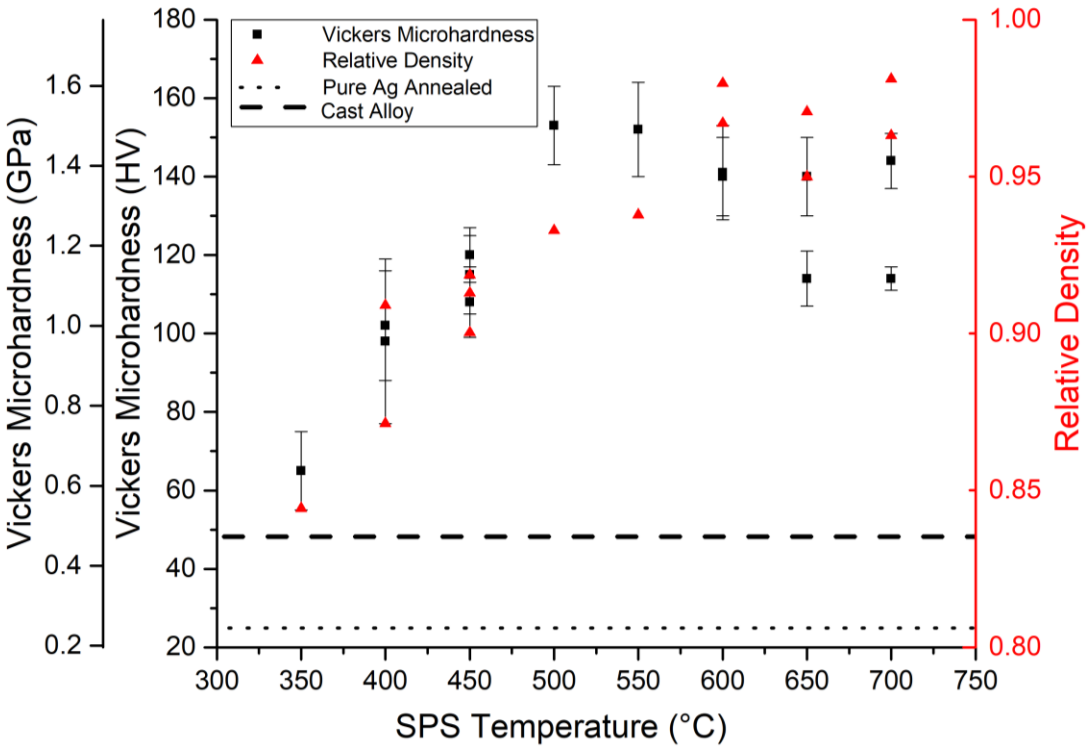

Figure 1: Hardness and density as a function of peak SPS temperature. Density is observed to increase with temperature; however, hardness is observed to peak between 500-550°C and soften at higher peak SPS temperatures. Multiple datapoints at equivalent temperatures come from samples with and without minor tungsten carbide contamination from the milling process.

2.3.2 Grain Size Relation to Vickers Hardness

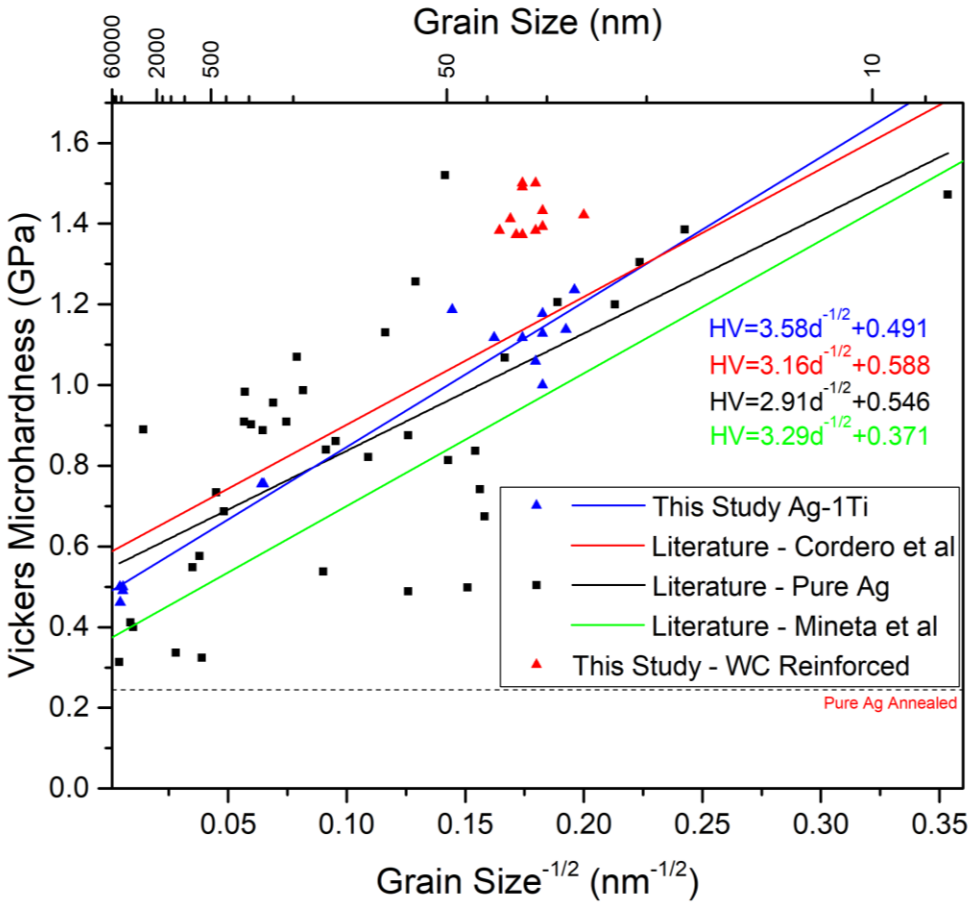

Figure 2: Hall-Petch relationship of pure silver from literature [15-24] overlaid with hardness and grain size data from cast Ag-1Ti samples and samples produced through MA and SPS. Hall-Petch parameters reported in studies by Cordero et al [9] and Mineta et al [34] are indicated in addition to parameters calculated in this study for pure Ag and Ag-1Ti.

Figure 2 displays a Hall-Petch plot constructed of hardness and grain size data of pure silver taken from literature, overlaid with data from this study. Data from literature is displayed in black. Data on NC silver from this study is displayed in blue, while data on NC silver reinforced with tungsten carbide (WC) dispersoids is displayed in red and does not follow the Hall-Petch trend. Hardness and grain size measurements of Ag-1Ti from this study for both mechanically alloyed and SPS processed samples, as well as cast samples, were analyzed in order to determine the Hall-Petch behavior of this alloy compared to that of pure silver. The cast Ag-1Ti samples

had a Vickers hardness of 0.49±0.02 GPa at a corresponding grain size of 41±9 μm, whereas the samples prepared by MA and SPS had a maximum hardness of 1.24±0.18 GPa at a corresponding grain size of 26nm, estimated by Scherrer's equation.

2.3.3 Effect of tungsten carbide contamination on Vickers hardness

Upon examination of the Ag-1Ti Hall-Petch data in Figure 2, a cluster of datapoints with a grain size of around 30nm and a Vickers hardness between 1.35-1.55GPa are observed to not fit the Hall-Petch approximation. The boost in hardness observed in these datapoints is attributed to Orowan strengthening caused by tungsten carbide contamination from breakdown of milling media during the MA process. At a grain size of around 30nm, these samples are found to have a Vickers hardness of nearly 300MPa higher than other datapoints at equivalent grain size. SEM analysis of the samples attributed with these datapoints (Figure 3) indicate that there are significant amounts of tungsten carbide within the matrix.

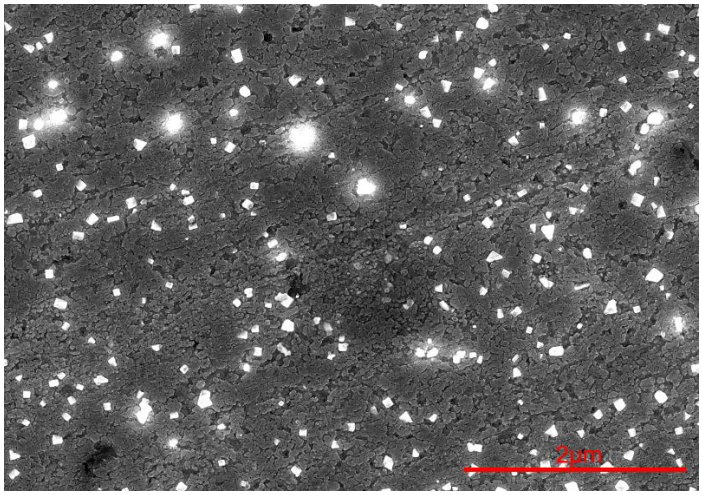

Figure 3: SEM BSE micrograph of tungsten carbide dispersoids from milling media within the Ag-1Ti matrix. WC particles are visible as light-colored angular particles within the darker Ag-1Ti matrix.

2.3.4 Effect of SPS Peak Temperature on grain size

XRD scans of Ag-1Ti samples SPS processed at various temperatures were analyzed using a full width at half maximum (FWHM) analysis with the Scherrer equation as confirmation

of the coarsening effect of elevated SPS temperature on grain size. XRD scans of pure unsintered silver precursor powder, cryomilled unsintered Ag-1Ti powder, and SPS processed Ag-1Ti samples sintered at peak temperatures of 500°C, 600°C, and 700°C are displayed in Figure 4, and estimated at a grain size of 26-38nm with the Scherrer equation at the Ag(111) peak. Broadening of the Ag peaks is observed between the initial unmilled Ag powder and the milled Ag-1Ti, indicating grain refinement in this alloy due to the MA process. Narrowing of the Ag peaks in the 500°C, 600°C, and 700°C conditions compared to the as-milled Ag-1Ti is indicative of grain coarsening occurring during SPS.

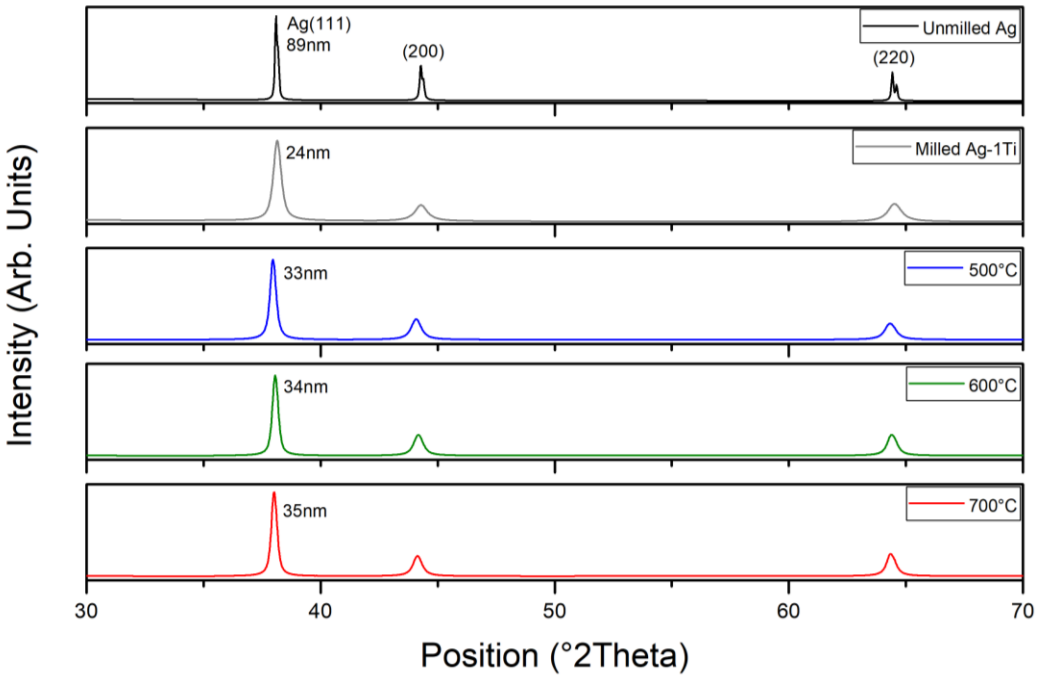

Figure 4: FWHM analysis of pure unmilled silver precursor powder, cryomilled Ag-1Ti powder, and Ag-1Ti SPS discs sintered at a peak temperature of 500°C, 600°C, and 700°C. Grain sizes estimates made by the Scherrer equation are shown beside the corresponding Ag(111) peaks for each condition.

2.3.5 Grain size verification by TEM

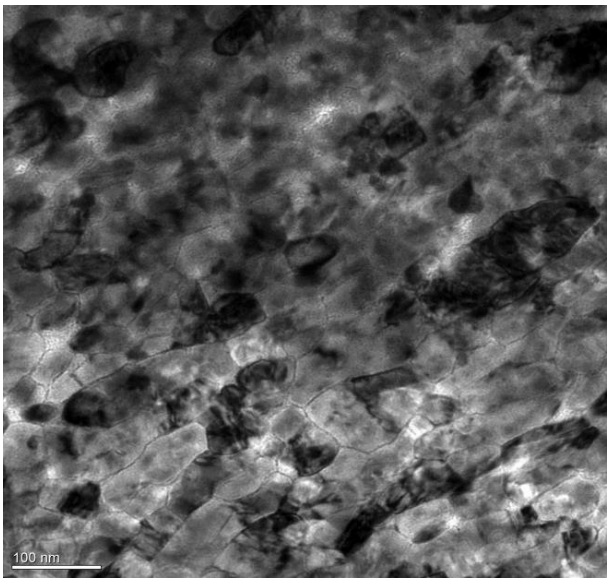

Figure 5: TEM verification of grain size estimated by XRD and Scherrer's equation. Grain size estimates by the line intercept method from this sample indicate a grain size of 31nm, confirming the grain size estimation of 33nm from XRD analysis.

Figure 5 displays a representative TEM micrograph of an Ag-1Ti SPS disc sintered at a peak temperature of 600°C. As the grain sizes in the sintered samples were too small to evaluate by SEM, grain size measurements made through XRD and the Scherrer equation were verified by TEM. The Scherrer equation was used to calculate an average grain size of 31nm for this sample; TEM verifies this estimation with a measured grain size of 33nm, calculated by the line intercept method.

2.4 Discussion

2.4.1 Strengthening Mechanisms Present in Ag-1Ti Processed by MA and SPS

The strength of metallic materials is determined by the level of applied stress necessary to overcome boundaries or obstacles within the microstructure which interfere with dislocation motion [25]. By processing this silver alloy through a combination of both MA and SPS there are several strengthening mechanisms that come into play through these processing methods. In

addition to the Peierls stress of pure silver, the Ag-1Ti alloy synthesized in this study is strengthened through solid solution strengthening by mechanical alloying with one percent titanium by weight. The MA process is also extremely effective at refining the grain structure of the particles through the severe plastic deformation induced by the milling process, introducing Hall-Petch strengthening into the alloy. The milling media used in this study is fabricated from sintered tungsten carbide with cobalt binder, which, although known for its exceptional hardness, is prone to fracturing and degradation during extended milling and leaves small particles behind in the milled powder [26]. As small pieces break off from both the WC milling vial and balls, they are ground into the silver matrix along with the titanium, further contributing to the strength of the alloy through the Orowan mechanism [27].

The strengthening mechanisms present in this alloy are described in the following section, and their individual strengthening contributions calculated to determine the relative strengthening contributed by each of the mechanisms. The summation of strengthening contributions to the hardness of this alloy may be considered as a summation of each of the individual contributions [15]:

$$H = H_0 + H_{SS} + H_{Oro} + H_{HP} \quad (1)$$

Where H indicates the overall hardness of the alloy, H_0 indicates the base hardness of silver due to Peierls stress of the lattice, H_{SS} indicates the hardness contribution due to solid solution strengthening with 1% Ti by weight, H_{Oro} indicates the hardness contribution due to the Orowan mechanism, and H_{HP} indicates the hardness contribution due to Hall-Petch strengthening.

2.4.2 Peierls Stress/Lattice Friction Stress of Pure Ag Matrix

Peierls stress, or lattice friction stress, is the most fundamental strengthening mechanism present in metallic materials and can be considered the strength of a metal in monocrystalline form, as it is the stress required to move a dislocation within a perfect crystalline lattice [28]. As

the matrix of metallic silver is an FCC structure with abundant slip systems present, dislocations may propagate along multiple present slip systems, resulting in a low Peierls stress relative to metals with other crystal structures. The Vickers hardness due to Peierls stress in pure silver in this case is assumed to be the same as the hardness of pure annealed silver at H_0=245MPa (25HV) [29] as indicated by the lower dashed line in Figure 2.

2.4.3 Hall-Petch/Grain Boundary Strengthening of Pure Ag vs. Ag-1Ti.

In this study, processing of precursor Ag-1Ti powder by MA serves two purposes. Firstly, the MA process is highly effective at homogenizing the alloy powder [30] through repeatedly fracturing and cold welding of the metal particles in the milling vial, effectively forcing the Ti powder into solution in the Ag powder. Secondly, MA is also highly effective as a grain refinement process, reducing the grain size of the Ag-1Ti powder through the same repeated fracturing and cold welding, causing increased dislocation density in the powder particles. As dislocation density in the lattice grows, dislocations eventually forms low angle grain boundaries which continue to absorb more dislocations, and, accompanied by grain rotation, decompose into finer grains separated by high angle grain boundaries [9].

By consolidating the milled Ag-1Ti powder with SPS, it is possible to synthesize bulk sintered material with NC grains, as the beneficial nanostructuring gained from the MA process is not lost through recrystallization during long holds at elevated temperatures common in traditional sintering processes [17]. Although the exact mechanism behind the SPS process is still under debate, fundamentally, the process combines aspects of sintering and hot pressing. The heating mechanism differs vastly from that of traditional sintering however, generating internal heating through Joule heating within the powder bed, rather than by external sources as is common in traditional sintering [31]. Localized high temperature and pressure hotspots between powder particle contact points give rise to enhanced sintering behavior compared to other

consolidation processes [32] and further aid in the densification of the powder [16]. These factors enable the production high density sintered samples within a relatively short timeframe (on the order of several minutes) and at lower temperatures and with shorter temperature ramp time than traditional sintering practices [33,34]].

The effect of SPS peak temperature on the grain size and relative density of Ag-1Ti SPS discs can be observed in Figure 1. The increase in hardness between peak temperatures of 350-550°C is attributed to an increase in density and interparticle sintering. Beyond 550°C density continues to increase at a reduced rate, however there is also an observed drop in hardness attributed to grain coarsening within the sintered discs between 550-700°C.

The measured hardness as a function of grain size is plotted as a modified version of the Hall-Petch equation (Equation 2) [15] in Figure 2 in order to determine the contribution of Hall-Petch strengthening to the overall strength and hardness of the alloy in Equation 1:

$$H = H_0 + kd^{-\frac{1}{2}} \quad (2)$$

Where H_{HP} is the contribution to the overall hardness of the alloy due to Hall-Petch strengthening, k is a strengthening coefficient, and d is the grain size [35]. According to the Hall-Petch relationship (Equation 2), the hardness as a function of grain size can be expressed as follows:

$$HV[GPa] = 2.91[GPa * nm^{0.5}]d^{-0.5} + 0.546[GPa]$$ (Pure silver from literature)

$$HV[GPa] = 3.58[GPa * nm^{0.5}]d^{-0.5} + 0.491[GPa]$$ (Ag-1Ti from this work)

The k value for pure silver is estimated at 2.91GPa*nm$^{1/2}$, while hardness measurements of this alloy indicate a k value of 3.58 GPa*nm$^{1/2}$, demonstrating that this alloy has improved hardenability when compared to pure silver samples from literature at equivalent grain sizes.

The contribution to the hardness in this alloy due to the Hall-Petch effect can be approximated by comparison of hardness of Ag-1Ti at a theoretical infinite grain size to the

hardness of Ag-1Ti at 25nm. From the Ag-1Ti Hall-Petch linear regression we can determine that the Ag1-Ti has a y-intercept of 491MPa, representing the hardness value of this alloy with no grain boundary strengthening. At a grain size of 25nm we can determine with Equation 2 that we should observe a Vickers hardness of 1.21GPa. Therefore, we can determine that at the smallest observed grain size, Hall-Petch strengthening contributes 716MPa.

2.4.4 Solid Solution Strengthening

The addition of 1% titanium by weight to this alloy contributes solid solution strengthening. The degree of strengthening attributed to the titanium addition is estimated through the Hall-Petch plot in Figure 2. The linear regressions of Ag-1Ti from this study indicate that in monocrystalline form, pure silver has a higher Vickers hardness than Ag1Ti. This is likely inaccurate due to the spread in the data, as it can be observed in Figure 2 at low grain sizes, the hardness of Ag-1Ti is higher than that reported of pure silver of comparable grain size.

Figure 2 indicates from the Hall-Petch relationship that pure Ag has a k value 2.91GPa*nm$^{1/2}$, whereas the k value of Ag-1Ti is 3.58GPa*nm$^{1/2}$. The data from these studies was used to determine an H_0 value of 0.546GPa, indicating that perfect monocrystal silver with no lattice strain or defects should have a hardness of 0.546GPa. This value is too large, which may be attributed to the scatter in data. The scatter is likely due to different processing and characterization methods used in different literature sources, which can produce distinct texturing or introduce different levels of impurities depending on the process [9]. Therefore, the hardness of pure annealed silver is substituted for an H_0 value of 0.245GPa [29]. The difference in hardness values between pure silver and Ag-1Ti with no grain boundary strengthening indicates that the overall contribution to hardness from solid solution strengthening with 1% titanium by weight is 246MPa.

2.4.5 Orowan Strengthening from WC Dispersoids

Tungsten carbide dispersoids from the MA process, visible in Figure 3, contribute to the overall hardness in this material by Orowan strengthening. Strengthening due to the Orowan mechanism can be calculated using Equations 3 and 4 [36]:

$$H_{Oro} = \frac{3\sqrt{3}Gb}{\lambda} \quad (3)$$

$$\lambda = 4r\frac{(1-f)}{3f} \quad (4)$$

Where G is the shear modulus of silver (28GPa), b is the Burgers vector for silver (0.289nm), r is the average nearest neighbor distance between WC particles (1.44μm) calculated from SEM micrographs, and f is the volume fraction of tungsten carbide within the Ag-1Ti matrix (3.50%) also calculated from SEM micrographs. From these values, the tungsten carbide dispersoids were calculated to increase the Vickers hardness of this material by 290MPa.

In Figure 2, two separate groupings of Ag-1Ti data points can be observed at a grain size of roughly 30nm – the lower grouping of hardness points is measured in samples with no tungsten carbide contamination; the upper grouping is indicated by the legend to be WC reinforced Ag-Ti. The Ag-1Ti grouping with a lower Vickers hardness is in agreement with the calculated Hall-Petch behavior, and samples from this grouping were found to have little to no tungsten carbide dispersoids and an average Vickers hardness of 1.13±0.07GPa. Ag-1Ti samples from the upper grouping were found to have a large degree of tungsten carbide contamination and an average Vickers hardness of 1.40±0.10GPa. The calculated hardness increase due to the Orowan mechanism is found to agree well with the difference in hardness observed in these two groupings, and adequately explains the significantly higher hardness compared to samples of equivalent hardness in the lower grouping of data points.

2.4.6 Total Calculated Strength

Contributions from each factor in the basic strengthening model for this material at a grain size of 25nm are outlined in Equation 1 is tabulated for each contribution in Table 1 below:

Table 1: Contribution to overall hardness by strengthening mechanism

Strengthening Mechanism	Vickers Hardness Contribution (MPa)
Peierls Lattice Friction H_0	245
Hall-Petch Strengthening H_{HP}	716
Solid Solution Strengthening H_{SS}	246
Orowan Dispersion Strengthening H_{Oro}	290
Total	1497

Contributions to strengthening are added linearly [37] to estimate the Vickers hardness of this alloy, calculated at 1.50GPa, which is in good agreement with the observed hardness values of 1.40±0.10GPa measured in samples with a grain size of 25nm and found to have tungsten carbide dispersoids present. The dominating mechanism in overall strengthening comes from the reduction of grain size in the alloy and is responsible for roughly half of the overall strength observed in the material. The near agreement of calculated and measured strength in this material indicates that the linear addition of the calculated strengthening contributions is an effective method for determining the theoretical strength of the alloy in the case of nanocrystalline Ag-1Ti.

2.5 Conclusions

A bulk nanocrystalline silver alloy was synthesized by cryomilling and SPS of pure silver and 1% by weight titanium precursor powders. Samples produced through this process were characterized by SEM, TEM and XRD and were subjected to Vickers indentation for hardness. The hardest observed samples were determined to have a grain size of between 25-38nm and fit into two distinct groupings on a Hall-Petch Plot. Samples with no tungsten carbide present displayed a Vickers hardness between 0.94-1.24GPa, and samples with tungsten carbide dispersoids from breakdown of milling media during cryomilling displayed Vickers hardness

between 1.37-1.50GPa. Contributions to strengthening were calculated based on strengthening mechanism theory for solid solution strengthening, grain boundary strengthening and Orowan strengthening from dispersoids, and compared to the hardness of bulk SPS processed samples. Theoretical calculations and measurements determined that the dominating strengthening mechanism present in this material is grain boundary strengthening, which contributes 716MPa, followed by Orowan strengthening, lattice friction stress and solid solution strengthening, which contribute 290, 245, and 246MPa respectively, in samples at a grain size of 25nm. The total experimentally observed Vickers hardness was an average of 1.4$\pm$0.10GPa, which is in good agreement with the theoretical total of 1.50GPa. This alloy shows promise as a high-strength, high-conductivity alternative material for electrical connectors and other applications that require both high conductivity and robust mechanical properties.

Acknowledgements

Erik Sease was supported in part by the Department of Education's Graduate Assistance in Areas of National Need (GAANN) fellowship. This research was supported by subcontract from QuesTek Innovations, LLC

Electron microscopy and microanalysis was performed on a ThermoFisher Scientific NNS450 and a ThermoFisher Scientific Titan Themis 300 in CFAMM at UC Riverside.

Conflicts of Interest: The authors declare no conflict of interest.

2.6 References

[1] Alexander, J. W. (2009). *History of the Medical Use of Silver. Surgical Infections, 10(3), 289–292.* doi:10.1089/sur.2008.9941

[2] Mijnendonckx, K., et al, (2013). *Antimicrobial silver: uses, toxicity and potential for resistance. BioMetals, 26(4), 609–621.* doi:10.1007/s10534-013-9645-z

[3] Praveen Kumar, S., et al, (2020). *Electrical and mechanical studies on pure-silver coated aluminium based electrical contact materials.* Materials Today: Proceedings. doi:10.1016/j.matpr.2020.05.666

[4] Mathaudhu, S. N., (2019). *Crystalline Metals Effortlessly Fit the Mold*. Physics, 12. doi:10.1103/physics.12.3

[5] S. Praiphruk, et al, *"Investigation of supersaturated silver alloys for high hardness jewelry application",* J. Met. Mater. Miner., vol. 23, no. 2, Dec. 2013.

[6] Goodrich, T., et al, (2014). *Performance testing and evaluation of a Ag-W nano-crystalline silver alloy as a gold replacement in electrical connectors.* 2014 IEEE 60th Holm Conference on Electrical Contacts (Holm). doi:10.1109/holm.2014.7031051

[7] Myers M., *Overview of the use of silver in connector applications.* Technical Paper, Interconnection & Process Technology Tyco Electronics, Harrisburg, PA. 2009 Feb 5:503-16.

[8] Sakai, Y., et al, (1992). *Development of a high strength, high conductivity copper-silver alloy for pulsed magnets.* IEEE Transactions on Magnetics, 28(1), 888–891. doi:10.1109/20.120021

[9] Cordero, Z. C., et al, (2016). *Six decades of the Hall–Petch effect – a survey of grain-size strengthening studies on pure metals. International Materials Reviews, 61(8), 495–512.* doi:10.1080/09506608.2016.1191808

[10] Meyers, M. A., et al, (2006). *Mechanical properties of nanocrystalline materials*. Progress in Materials Science, 51(4), 440. doi:10.1016/j.pmatsci.2005.08.003

[11] Enayati, M. H., & Mohamed, F. A. (2014). *Application of mechanical alloying/milling for synthesis of nanocrystalline and amorphous materials.* International Materials Reviews, 59(7), 394–416. doi:10.1179/1743280414y.0000000036

[12] Kozlík, J., et al, (2018). *Cryogenic Milling of Titanium Powder.* Metals, 8(1), 31. doi:10.3390/met8010031

[13] Fieberg, M., et al, (2003). *Silver, Gold, and Other Noble Metals. Digital Encyclopedia of Applied Physics.* doi:10.1002/3527600434.eap437

[14] Liu, D., et al, (2011). *Spark Plasma Sintering of Cryomilled Nanocrystalline Al Alloy - Part II: Influence of Processing Conditions on Densification and Properties*. Metallurgical and Materials Transactions A, 43(1), 340–350. doi:10.1007/s11661-011-0841-6

[15] Kizuka, T. et al, *Structure and Hardness of Nanocrystalline Silver,* (1997). *Journal of Materials Science, 32(6), 1501–1507.* doi:10.1023/a:1018566303784

[16] Ng, H. B., et al, (2007). *Spark plasma sintering of silver nanopowder. BioMEMS and Nanotechnology III.* doi:10.1117/12.759383

[17] Wang, H., et al, (2016). *Microstructures and mechanical properties of bulk nanocrystalline silver fabricated by spark plasma sintering.* Journal of Materials Research, 31(15), 2223–2232. doi:10.1557/jmr.2016.212

[18] G.W. Nieman et al, (1992). *Mechanical Behavior of Nanocrystalline Metals*, Nanostructured Materials Vol. 1, pp. 185-190, 1992.

[19] X.Y. Qin et al, (1995). *The Microhardness of Nanocrystalline Silver*, NanoStructured Materials, Vol. 5, No 1, pp. 101-110, 1995.

[20] I. Marek et al, (2015). *High-Strength bulk nano-crystalline silver prepared by selective leaching combined with spark plasma sintering*, Materials Science & Engineering A 627 (2015) 326–332.

[21] L. Zhang et al, (2008). *Fabrication of bulk nanostructured silver material from nanopowders using shockwave consolidation technique*, Materials Science and Engineering A 487 (2008) 219–227.

[22] J. Gubicza et al, (2010). *Principles of self annealing in silver processed by equal-channel angular pressing*, Materials Science and Engineering A 527 (2010) 752–760.

[23] J. Xu et al, (1997). *Nanocrystalline Ag Formed by low-temperature high-energy mechanical attrition*, Nanostructured Materials, Vol. 8 No. 1, pp. 96, 1997

[24] Kobelev, N. P., et al, (1993). *Microhardness and elastic properties of nanocrystalline silver.* Nanostructured Materials, 2(5), 537–544. doi:10.1016/0965-9773(93)90171-7

[25] Huskins, E. L., et al, 2010). *Strengthening mechanisms in an Al–Mg alloy.* Materials Science and Engineering: A, 527(6), 1292–1298. doi:10.1016/j.msea.2009.11.056

[26] J. Kozlik et al, (2018). *Cryogenic Milling of Titanium*, Metals 2018, 8, 31; doi:10.3390/met8010031

[27] Kendig, K. L., Miracle, D. B. (2002). *Strengthening mechanisms of an Al-Mg-Sc-Zr alloy.* Acta Materialia, 50(16), 4165–4175. doi:10.1016/s1359-6454(02)00258-6

[28] Lubarda, V.A., Markenscoff, X., (2007). *Configurational force on a lattice dislocation and the Peierls stress.* Arch Appl Mech **77,** 147–154 (2007). https://doi.org/10.1007/s00419-006-0068-y

[29] ASTM B413-97a(2017), Standard Specification for Refined Silver, ASTM International, West Conshohocken, PA, 2017, www.astm.org

[30] C. Suryanarayana, *Mechanical alloying and milling*, Progress in Materials Science, Volume 46, Issues 1–2, 2001, Pages 1-184, ISSN 0079-6425, https://doi.org/10.1016/S0079-6425(99)00010-9.

[31] Guillon, O., et al, (2014). *Field-Assisted Sintering Technology/Spark Plasma Sintering: Mechanisms, Materials, and Technology Developments.* Advanced Engineering Materials, 16(7), 830–849. doi:10.1002/adem.201300409

[32] Munir, Z. A., et al, (2006). *The effect of electric field and pressure on the synthesis and consolidation of materials: A review of the spark plasma sintering method.* Journal of Materials Science, 41(3), 763–777. doi:10.1007/s10853-006-6555-2

[33] Zhu, K. N., et al, (2017). *Microstructure and mechanical strength of near- and sub-micrometre grain size copper prepared by spark plasma sintering.* Materials & Design, 117, 95–103. doi:10.1016/j.matdes.2016.12.042

[34] Mineta, T., et al, (2019). *Structure and mechanical properties of nanocrystalline silver prepared by spark plasma sintering.* Materials Science and Engineering: A, 754, 258–264. doi:10.1016/j.msea.2019.03.101

[35] Naik, S. N., & Walley, S. M. (2019). *The Hall–Petch and inverse Hall–Petch relations and the hardness of nanocrystalline metals*. Journal of Materials Science. doi:10.1007/s10853-019-04160-w

[36] J. Moon et al, (2008). *Orowan strengthening on the effect of the nanoindentation hardness of the ferrite matrix in micro-alloyed steels*, Materials Science and Engineering A 487 (2008) 552-557, DOI:10.1016/j.msea.2007.10.046

[37] Wen, H., et al, (2013). *Strengthening mechanisms in a high-strength bulk nanostructured Cu–Zn–Al alloy processed via cryomilling and spark plasma sintering*. Acta Materialia, 61(8), 2769–2782. doi:10.1016/j.actamat.2012.09.036

Chapter 3: Electrical and Mechanical Properties of Ultrafine Grained Thermally Stable Dilute Silver Alloys Processed by High Pressure Torsion

3.0 Abstract

Severe plastic deformation processing of 3N purity silver and two dilute silver alloys is explored through high pressure torsion, producing high strength silver in bulk form. Samples produced by this process are characterized by indentation and tensile testing to explore their mechanical properties, and the effects of processing and alloying on the electrical conductivity is investigated with a 4-point conductivity probe. Characterization via SEM before and after long-term storage reveals an ultrafine grained microstructure with excellent thermal stability. This work promises bulk high strength silver alloys with exceptional electrical conductivity, resistant to self-annealing and grain growth at ambient temperature.

3.1 Introduction

Bulk nanocrystalline (NC) and ultrafine-grained (UFG) materials have gained a considerable amount of interest in the last several decades due to the extraordinary properties that they exhibit compared to their coarse-grained counterparts [1]. In particular, mechanical properties are found to significantly increase with reduction of grain size to the nanometer level [2]. Due to their small grain sizes, NC (<100 nm average grain size) and UFG (100 – 1000 nm average grain size) materials often have poor microstructural stability at elevated temperatures [3] due to the strong driving force favoring recrystallization caused by the high surface area to volume ratio of nanometer scale grains. This recrystallization is a roadblock for their practical use, as this instability causes grain growth and loss of high hardness and strength. Many NC and UFG materials have been shown to be stable against grain coarsening at elevated temperatures, however this is often accomplished through alloying to reduce excess grain boundary energy and kinetically pin grain boundaries with solutes, or lower energy crystallographic features such as

twin boundaries [4, 5]. Some pure metals such as silver and copper are found to be unstable at low homologous temperatures and will even undergo self-annealing and grain growth at ambient temperature [6]. Silver in particular has been found to undergo rapid self-annealing and loss of mechanical properties at room temperature, in part due to its extremely low stacking fault energy (SFE) [7].

A common method of reducing grain sizes in metals is by severe plastic deformation (SPD). SPD processing techniques are a family of processing techniques for metals which utilize the application of immense strain within a constrained die to generate hydrostatic pressure and prevent free flow of the material. By preventing free flow, it is possible to introduce increased level of grain refinement and defect density into materials without causing significant change in the net geometric shape [8]. Through these processes, the grain size can be reduced to the NC or UFG regime, producing materials with higher strength or hardness through the Hall-Petch strengthening [9] than is possible by conventional forming processes.

In previous studies on SPD processing of high purity silver [3, 10, 11], it has been noted that the low stacking fault energy of silver allows for accumulation of extremely high dislocation densities [12]. This is due to the tendency of dislocations to dissociate into partial dislocations in low SFE materials, impeding dislocation annihilation and increasing dislocation density compared to materials with higher SFEs. This high degree of dislocation density in silver, combined with the high volume fraction of defects and grain boundaries when processed by SPD methods, yields a higher driving force toward recovery and recrystallization, causing self-annealing and grain growth of silver within days of processing by SPD [11] and loss of mechanical properties. Despite this tendency to self-anneal, it has been shown that a small reduction of the purity level of silver has a significant effect on its stability. In a study by Hegedus et al [13], 99.995% (4N5) purity silver processed by 16 passes of equal channel angular

pressing (ECAP), another SPD process, was found to undergo self-annealing after 4 months in ambient storage and a loss in hardness of over 500 MPa. By reducing the purity to 99.99% (4N), the loss in hardness was reduced to just over 100 MPa after identical processing and storage conditions.

While the addition of impurities or alloying additions is an attractive option to increase the thermal stability of alloys by kinetic pinning of grain boundaries by solutes or increasing the SFE, even a small amount of alloying addition can significantly reduce the electrical conductivity [14]. Silver is well known for its excellent electrical conductivity, however alloying significantly reduces this. By alloying with 7.5 percent copper by weight to produce sterling silver, one of the most common silver alloys, the electrical conductivity is reduced to only 88% of that of pure silver [15]. This large reduction in conductivity reduces the attractiveness of alloyed silver in electrical applications, therefore a balance of strengthening and stabilization with low levels of alloying additions to avoid reductions in conductivity are imperative in applications where high conductivity is preferred.

In this study, lower purity 3N silver and two dilute silver alloys were cast and processed by high pressure torsion (HPT). Characterization through electron microscopy, x-ray diffraction, indentation and tensile testing is utilized to determine the effect of reduced purity and alloying additions, and the effect of time and varying levels of strain on the long-term mechanical properties, electrical conductivity, and grain size stability of silver. Through the addition of impurities and dilute alloying additions, we aim to produce high strength, high conductivity silver and silver alloys with significant long-term thermal stability.

3.2 Methods and Materials

3.2.1 Materials and Processing

Buttons of ~15 grams were cast from 99.9% (3N) purity silver, Ag-1Ti, and Ag-1Cu-1Pt (weight percent) in a vacuum induction melter and allowed to homogenize and form a complete solid solution under inert atmosphere. Homogenization was performed at 900°C for 72 hours for the 3N Ag, 900°C for 96 hours for the Ag-1Ti, and 750°C for 90 hours for the Ag-1Cu-1Pt. After solidification, the buttons were sectioned via wire electrical discharge machining (Sodick, Schaumburg, IL) to produce sections 1.5 mm thick. Disc shaped samples 10mm in diameter were then cut from the sections and mechanically thinned to 1.2 mm thickness for HPT processing. Two discs of pure silver, two discs of Ag-1Ti and three discs of Ag-1Cu-1Pt were produced, and grain size measurements were performed via light optical microscopy. Two discs from each silver alloy were subjected to HPT at room temperature and 1 RPM with 4 GPa for 4 and 6 turns each, and the extra Ag-1Cu-1Pt disc was subjected to 10 turns at otherwise identical parameters to determine the effect of varying strain on the alloys (Table 1). The 6-turn* pure silver disc was briefly exposed to 4.6 GPa during an over-correction of pressure but was otherwise processed at identical parameters as the other samples. The results of this over-pressurization are indicated with an asterisk* in this work so as to distinguish them from the normally processed material.

The processed discs were mechanically ground and then polished to a mirror finish with a 50nm alumina suspension for microstructural characterization with x-ray diffraction (XRD) and microhardness measurements, detailed in section 2.2 below. To determine the long-term stability behavior of the processed material, the samples were stored at room temperature for 36 months, then repolished, followed by the same routes of characterization as well as scanning electron microscopy (SEM) with concentric backscatter (CBS) for direct grain size measurement.

After microstructural characterization was completed post-storage, wire EDM was used to cut two small-scale dogbone tensile samples from each HPT disc, with a gauge width and length of 1 mm and 3 mm respectively, and a gauge thickness of roughly 1 mm (Figure 1). The gauge section of each sample was cut out from the processed discs at a distance between 1.75-2.55 mm from the center. Two small-scale dogbone samples were also cut from the remnants of the pure silver button for determining baseline mechanical and electrical properties before processing by HPT.

Table 1: Parameters of Samples Processed by HPT

Alloy	Number of HPT Turns	HPT Pressure (GPa)	As-Cast Vickers Microhardness (MPa)
3N Ag	4	4	432±27
3N Ag*	6	4 + 0.6	432±27
Ag-1Ti	4	4	608±51
Ag-1Ti	6	4	608±51
Ag-1Cu-1Pt	4	4	569±21
Ag-1Cu-1Pt	6	4	569±21
Ag-1Cu-1Pt	10	4	569±21

Figure 1: 10mm diameter silver alloy disc post-HPT with two small-scale dogbone samples.

3.2.2 Microhardness and Microstructural Characterization

Hardness of buttons in the as-cast condition was evaluated by microindentation with a Phase II Vickers Micro Hardness Tester at a load of 200 g and a dwell time of 15 seconds to determine a baseline hardness for each alloy, and grain size was measured via light optical microscopy and the line intercept method. After HPT processing, hardness was re-evaluated via

indentation: Three lines of indents at 60° relative to each other were placed with indents at spacings of 3 mm across the diameter of the samples, providing hardness of the discs as a function of radial distance. Equivalent von Mises strain due to the severe plastic deformation of the HPT process was calculated using Equation 1 [16], given the number of revolutions of HPT, N, radial distance from the center of the HPT disc, r, and the original height of the disc, h.

$$\varepsilon_{Eq} = \frac{2\pi Nr}{h\sqrt{3}} \quad (1)$$

To estimate the grain size of the discs after HPT processing, XRD scans were performed on the discs in a PANalitycal Empyrean Series 2 XRD, and grain size was estimated by Scherrer's equation using a full-width half maximum estimation of the Ag(111) peak.

After 36 months in ambient air storage, the HPT processed discs were reevaluated via microindentation with the same methods in order to determine the long-term stability of the microstructures and mechanical properties. SEM imaging with CBS was performed on a NNS450 SEM to determine grain size of the discs via the line intercept method at half radius of the discs (2.5 mm from the center).

3.2.3 Conductivity Measurements

The surfaces of the dogbone samples were re-polished with the same methods as previously mentioned to remove any surface irregularities and oxide contamination. Conductivity measurements were performed on the gauge section of the micro-scale tensile samples after polishing with the 4-wire resistance test method [12] using a Keithley 2636B System SourceMeter. A source current of 1A was passed through two source leads positioned on the grip section of the dogbones and the voltage was measured between two sense leads positioned at either end of the gauge section of the dogbones (Figure 2). The current reversal method [12] was used to cancel out thermoelectric voltages generated by thermal gradients and dissimilar metals within the circuitry of the Keithley SourceMeter and the 4-point probe, therefore isolating the

measured voltage within the material. Five conductivity measurements were performed per dogbone sample, with ten samplings performed per measurement to determine an average conductivity value for each dogbone.

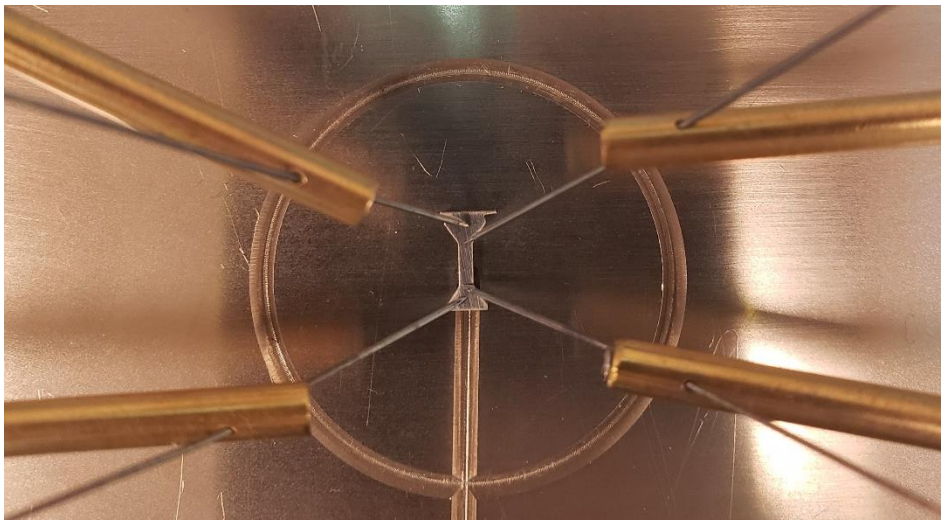

Figure 2: 4-Point conductivity probe leads positioned on a small-scale dogbone tensile sample. Source leads are positioned at the top and bottom of the sample, and sensing leads are positioned in the center.

3.2.4 Small-Scale Tensile Testing

Tensile testing was performed on the HPT-processed dogbone tensile samples in a Instron 5969 Dual Column load frame at an initial strain rate of 10^{-2} s^{-1} to evaluate the response in mechanical properties of the HPT processed material compared to the unalloyed and unprocessed material. To accurately determine stress and strain data, load on the specimen was measured via the loadcell on the load frame at a sample rate of 30 measurements per second. Strain on the tensile samples was determined via a digital image correlation (DIC) system using a Sony a7 III camera with a Venus Laowa 24mm f/14 macro probe lens filming the extension of the samples at a framerate of 30 fps. Prior to testing, the surface of the dogbone samples was painted with a thin layer of white acrylic paint, over which they were lightly speckled with black paint to provide a high resolution and high contrast surface lattice of black points on a white background. Displacement of each point relative to its neighbors was used to determine the strain on the

samples as a function of time using open source DIC software GOM Correlate and was synced to the load data to provide stress-strain data for each tensile sample.

3.3 Results

3.3.1 Microstructural Characterization

Grain size and average Vickers microhardness measurements of the material via different characterization routes are indicated in Table 2: Light optical microscopy measurements of the as-cast material pre-processing, XRD Scherrer's analysis measurements from pre-storage, and SEM measurements from post storage taken at half radius are reported. XRD grain size measurements of the as-processed material was not validated via electron microscopy (Figure 3), and was determined to be inaccurate when compared with the SEM measurements. This is due to the upper limit of grain sizes measurable by Scherrer's equation, which is only accurate for grain sizes under 100nm [17]. Grain size values from literature indicate a grain size of 230±30 nm for of 4N silver directly after processing by 1 turn of HPT at 6 GPa, which is in good agreement with grain size values estimated by SEM after storage [18]. An SEM micrograph of the 4-turn Ag-1Ti microstructure at half radius

Table 2: Grain size of samples processed by HPT. Post-storage SEM grain size measurements were performed at half radius

Alloy	Number of HPT Turns	As-Cast Grain Size (μm)	XRD Est. Grain Size Pre-Storage (nm)	SEM Avg. Grain Size Post Storage (nm)	Pre-Storage Vickers Microhardness (MPa)	Post-Storage Vickers Microhardness (MPa)
3N Ag	4	508	61	222±10	745±37	760±39
3N Ag*	6	508	56	209±41	934±65	925±96
Ag-1Ti	4	296	58	243±6	749±31	770±36
Ag-1Ti	6	296	54	237±32	769±30	765±40
Ag-1Cu-1Pt	4	439	51	185±48	782±61	733±76
Ag-1Cu-1Pt	6	439	56	190±41	849±27	808±27
Ag-1Cu-1Pt	10	439	50	196±41	810±53	794±40

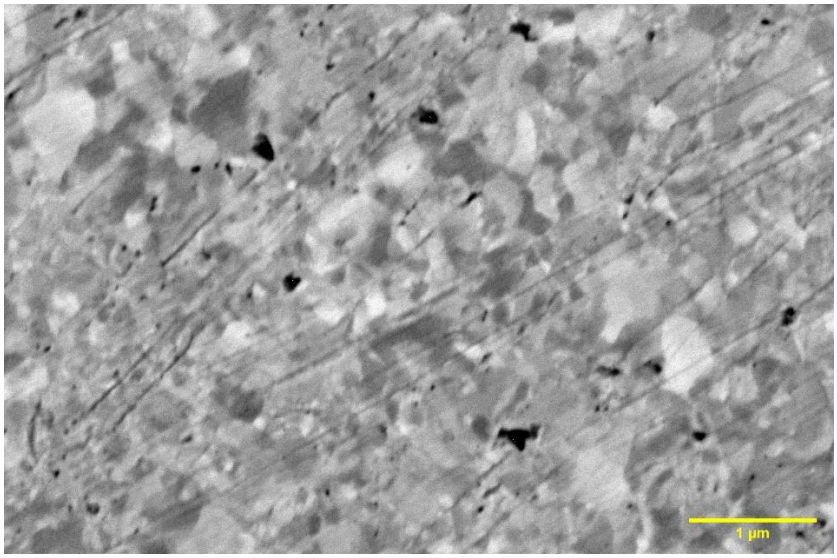

Figure 3: A representative SEM with CBS micrograph used for grain size analysis, taken at half radius on the 4-turn Ag-1Ti sample with an accelerating voltage of 5kV and spot size of 3µm.

3.3.2 Hardness as a Function of Equivalent Strain

Hardness of the silver HPT discs before and after 36 months of room temperature storage was evaluated via indentation as a function of equivalent strain to determine if self-annealing, grain growth and softening of the material had occurred during storage. By plotting hardness as a function of equivalent strain, it is possible to visualize the effects of the number of HPT turns as well as the effect of radial distance on the strain gradient within the material, and by extension the effect of both on the hardness of the material. Figure 4 displays the Vickers microhardness as a function of equivalent strain for discs of 3N Ag, Ag-1Ti, and Ag-1Cu-1Pt processed by different number of HPT turns, before and after 36 months in ambient temperature storage. The lower dashed line on each plot indicates the hardness of the as-cast material prior to HPT processing.

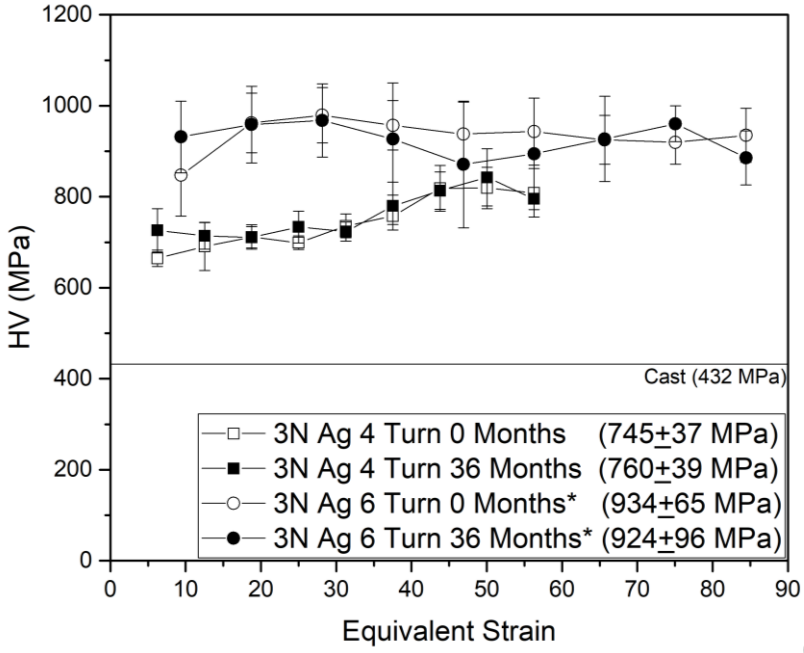
HV (MPa)
Equivalent Strain
Cast (432 MPa)
3N Ag 4 Turn 0 Months (745±37 MPa)
3N Ag 4 Turn 36 Months (760±39 MPa)
3N Ag 6 Turn 0 Months* (934±65 MPa)
3N Ag 6 Turn 36 Months* (924±96 MPa)

(a)

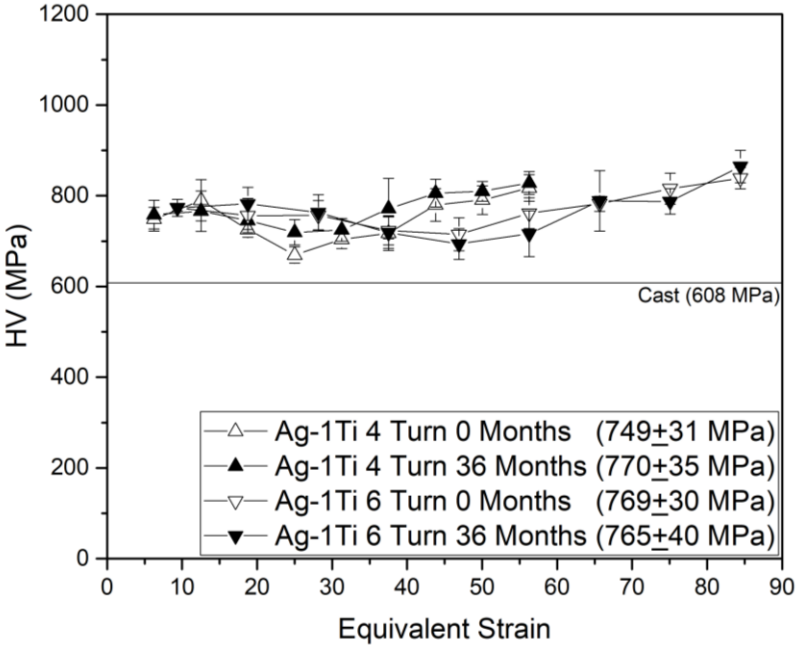
HV (MPa)
Equivalent Strain
Cast (608 MPa)
Ag-1Ti 4 Turn 0 Months (749±31 MPa)
Ag-1Ti 4 Turn 36 Months (770±35 MPa)
Ag-1Ti 6 Turn 0 Months (769±30 MPa)
Ag-1Ti 6 Turn 36 Months (765±40 MPa)

(b)

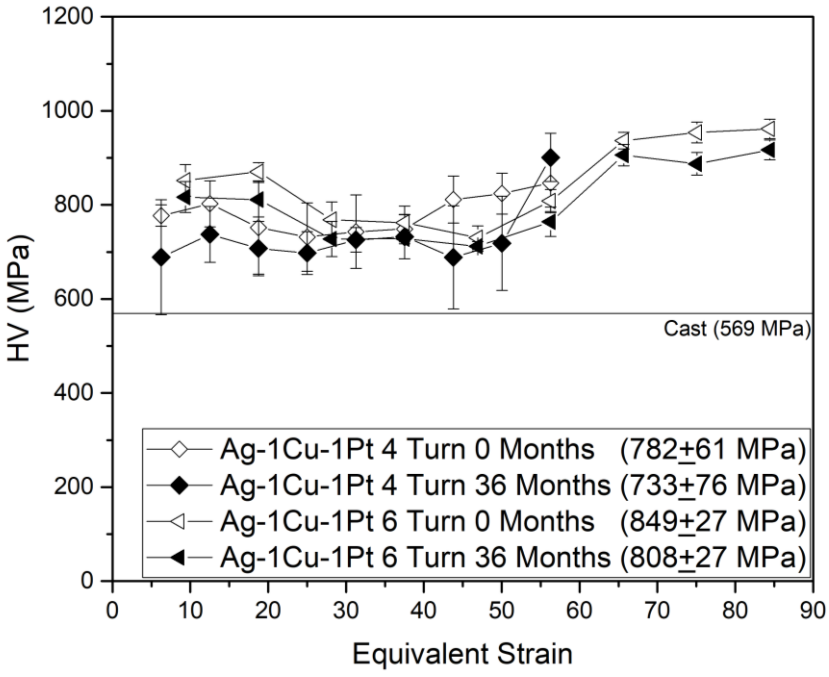

(c)

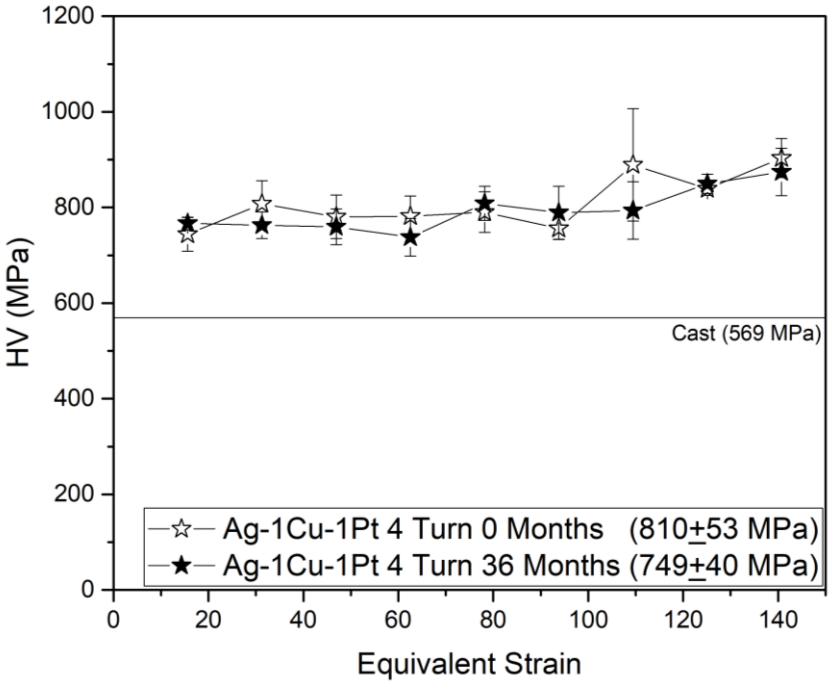

(d)

Figure 4: Hardness as a function of equivalent strain for a) 99.9% purity silver processed by 4 and 6* turns, b) Ag-1Ti processed by 4 and 6 turns, c) Ag-1Cu-1Pt processed by 4 and 6 turns, and d) Ag-1Cu-1Pt processed by 10 turns of HPT before and after 36 months of storage at room temperature. The 10-turn sample is plotted separately for ease of visibility.

From Figure 4 it can be observed that the HPT process yielded an increase in hardness from the cast state across the entire range of strain that the samples were subjected to. Hardness was generally found to increase according to increasing levels strain, due to both increasing the number of turns of HPT and increase in radial distance.

The highest increase in hardness from the as-cast state to the original HPT processed state was observed in the 6-turn* 3N purity silver sample, where hardness increased by an average Vickers microhardness of 502 MPa from the as cast condition. The Ag-1Ti and Ag-1Cu-1Pt samples were both observed to have comparatively smaller increases in harness from the as-cast state to the HPT processed state in comparison to the 6-turn* 3N Ag. The Ag-1Ti 6-turn sample saw an average increase in hardness from the as-cast state of 161 MPa, and the Ag-1Cu-1Pt 6-turn sample saw a maximum increase in Vickers hardness of 280 MPa. Overall, these increases in hardness account for an increase of 216%*, 127% and 149% from the as cast condition of the 3N Ag, Ag-1Ti and Ag-1Cu-1Pt samples respectively.

The silver and silver alloys processed by HPT were found to be stable across all levels of strain that the samples were exposed to, with most samples seeing only a slight reduction in the hardness over the time in room temperature storage. The largest loss in hardness was observed in the 4-turn Ag-1Cu-1Pt sample, which saw an average Vickers microhardness reduction of 49 MPa during storage, while the greatest average hardness reduction in the other alloys occurred in the 6-turn* 3N silver and 6-turn Ag-1Ti samples, at 9 MPa and 4 MPa, respectively.

Some discs were found to increase in hardness after storage; an unanticipated result, as the processed material was expected to self-anneal due their high dislocation density and strain, and the low SFE of silver [3]. Both the 4-turn 3N Ag and 4-turn Ag-1Ti discs were observed to increase in hardness across most of the range of strains they were subjected to, however the increases lie within a standard deviation of the average hardness value.

In the 3N silver samples, a vast difference in hardness is observed at the same values of equivalent strain for the 6-turn* 3N sample versus the 4-turn 3N sample. This difference is believed to be due to the over pressurization during processing, as the equivalent strain should be similar when accounting for both number of turns and radial distance, and therefore yield a similar microhardness value, as observed in the other samples.

3.3.3 Electrical Conductivity

Electrical conductivity and mechanical properties from testing performed on dogbone samples prior to tensile testing are reported in Table 3 below. Electrical conductivity is reported as a percentage of the International Annealed Copper Standard (IACS), where 100% IACS is equal to 58 MS/m, the conductivity of annealed commercially available copper [19]. As silver possesses a higher electrical conductivity than copper at 105%, it is not uncommon to see electrical conductivity values for silver expressed as over 100% IACS.

Conductivity was found to depend largely on the alloy used, with little variance due to processing conditions. As the grain sizes between the processed samples is similar (212$\pm$35nm), most of the discrepancy in conductivity is believed to be dependent on the alloying additions used, rather than by scattering at grain boundaries or other lattice defects. The 3N silver samples processed by HPT were found to have the highest conductivity of all the processed samples at between 97-100% IACS, with little to no reduction in conductivity compared to the as-cast condition. The Ag-1Cu-1Pt alloy samples also displayed good conductivity between 86-91% IACS, with little variation due to processing conditions, while the Ag-1Ti alloy samples displayed the lowest conductivity at 60-62% IACS. The conductivity of the Ag-1Cu-1Pt samples were also found to increase with increasing number of turns, counterintuitive to the expected drop in conductivity with an increase in strain and electron scattering sites within the metal lattice.

Table 3: Conductivity and conductivity of silver and silver alloys processed by HPT. Data from two tensile samples cut from the as-cast 3N Ag are also included. All values indicate average and standard deviation of properties measured from the two dogbone tensile samples cut from each disc, except for the mechanical properties of the 4-turn Ag-1Cu-1Pt which saw a failure in one of the samples during mechanical testing.

Alloy	Number of HPT Turns	Electrical Conductivity (%IACS)	0.2% YS (MPa)	UTS (MPa)	Elongation to Failure (%)
3N Ag	As-Cast	99.6±1.1	49±9	121±1	54±4
3N Ag	4	99.1±0.9	148±5	180±7	29±1
3N Ag	6*	97.5±0.9	141±2	218±15	36±4
Ag-1Ti	4	61.3±0.2	153±8	167±2	30±4
Ag-1Ti	6	61.5±0.4	164±12	176±5	24
Ag-1Cu-1Pt	4	86.9±0.5	113	125	15
Ag-1Cu-1Pt	6	89.7±1.0	131±3	152±7	20±3
Ag-1Cu-1Pt	10	89.8±0.7	154±2	158±3	26±3

3.3.4 Mechanical Testing

Figure 5 displays the engineering stress-strain curves of the tensile samples prepared from the processed HPT discs and unprocessed 3N Ag button. The yield strength (0.2% flow stress), ultimate tensile strength (UTS), and elongation to failure are reported in Table 3. Samples processed by HPT show considerable strengthening compared to the as-cast condition, displaying an increase of UTS and yield strength with increasing number of turns, consistent with the general increase in Vickers microhardness seen with increasing equivalent strain.

The highest average yield strength observed in any of the HPT processed samples was 164 MPa in the 6-turn Ag-1Ti material, amounting to 338% increase in yield strength compared to the average yield strength seen in the as-cast 3N purity silver. The highest UTS observed in the HPT processed material was seen in the 6-turn* 3N Ag, which displayed an average UTS of 218 MPa; 180% increase in comparison to the as-cast material.

Elongation to failure was found to decrease for all samples compared to the as-cast condition, which is consistent with the loss in elongation commonly seen in NC and UFG

materials, which are often found to fail at 5-10% elongation [20]. Good elongation is still retained in the material processed by HPT however, with a maximum average elongation of 36% observed in the 6 turn 3N Ag* samples, although this is believed to be in part due to over pressurization of this sample.

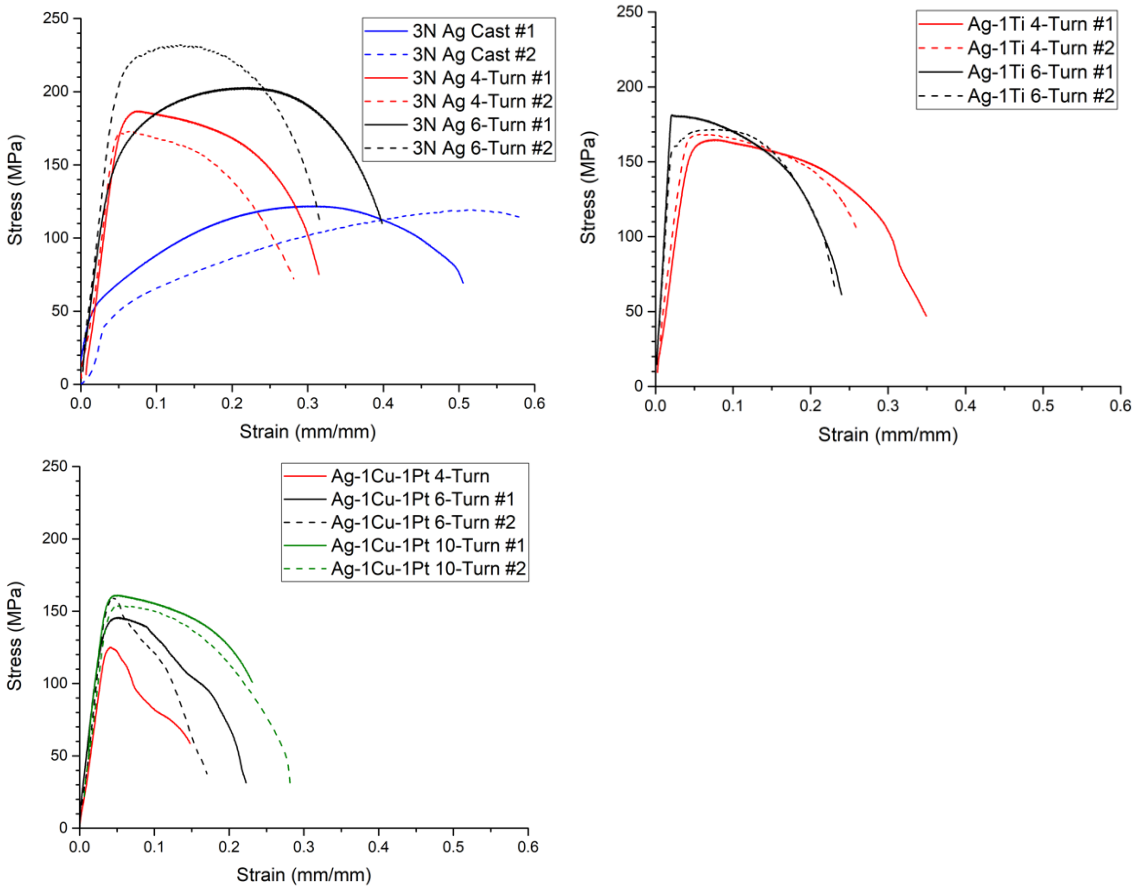

Figure 5: Engineering stress-strain plots of a) 99.9% purity Ag as-cast and processed by HPT, b) Ag-1Ti processed by HPT, and c) Ag-1Cu-1Pt processed by HPT.

Figure 6 displays yield stress normalized by shear modulus as a function of electrical conductivity, plotted from data from a study by X. Ke et al [21]. Data is reported for NC, UFG and coarse-grained metals, overlaid with data from the UFG silver from this study. Despite the relative softness of silver compared to many other structural metals, UFG silver processed by

HPT from this study was found to display excellent electrical conductivity, especially in the 3N purity silver samples, which are only surpassed in electrical conductivity by coarse-grained Cu and Ag. Ag-1Ti processed by HPT, while displaying the poorest electrical conductivity of all the material evaluated in this work, still displays a balance of mechanical properties and electrical conductivity rivalling that of UFG aluminum [21]. It is also worth mentioning that many of the best performing materials, namely the nanotwinned and nanocrystalline silver (NC+NT Ag) and nanotwinned silver and copper (NT Ag+Cu) are only produced in thin film form [21], while HPT material from this study is produced in bulk form.

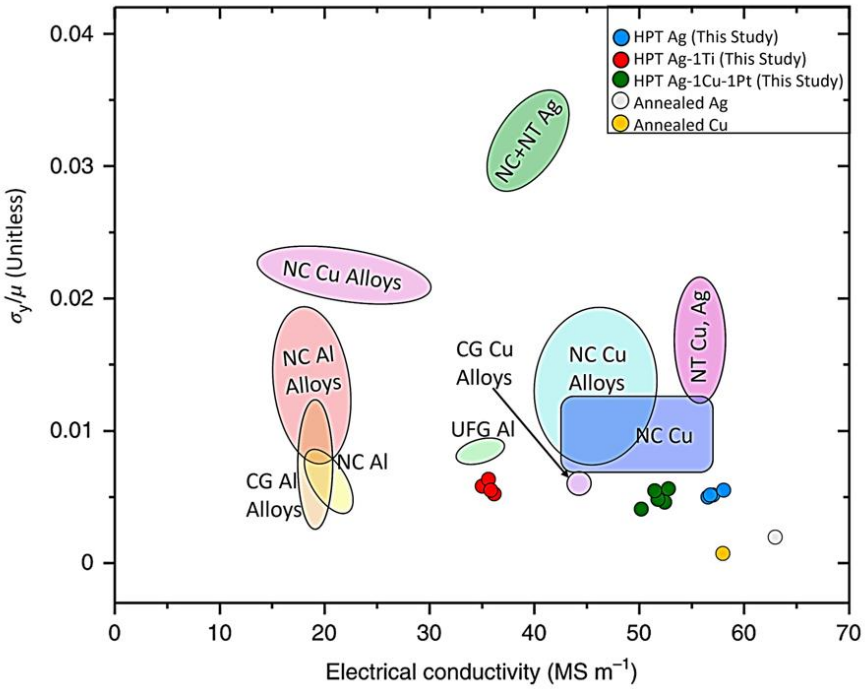

Figure 6: Yield strength normalized by shear modulus (σ_y/μ) as a function of electrical conductivity for common metals and metal alloys used for electrically conducting applications; data from Ref. [21], with electrical conductivity and yield strength data from bulk UFG HPT silver and silver alloys from this study. The annealed copper and annealed silver points correspond to 100 and 105% AICS respectively.

3.4 Discussion

3.4.1 Room Temperature Self-Annealing Behavior

In prior studies on SPD processing of silver, it has been noted that self-annealing in silver begins within a very short period of time after processing. In a study by Gubicza et al [3] on the self-annealing behavior at room temperature of 4N5 silver processed by different numbers of passes of ECAP, self-annealing and significant loss of mechanical properties occurred within 1 month after processing by 4, 8 and 16 passes of ECAP, determined by microhardness measurements on the samples. Within 4 months of storage after ECAP processing, the Vickers hardness of the 4-pass sample had dropped by roughly 250 MPa, and the 8 and 16 pass samples by roughly 500 MPa.

In a similar study by Matsunaga and Horita on SPD processing of fcc metals by HPT [10], 4N purity silver processed by 5 turns of HPT at 6 GPa was found to decrease in hardness after only 1.5 days when stored at room temperature. Larger reductions in hardness were observed in regions of the samples exposed to higher levels of strain, indicating that strain energy imparted by the HPT process was a driving force for the observed reduction in hardness [9]. The large loss in mechanical properties observed in high purity silver is considered to be due to the extremely low SFE in silver, allowing the accumulation of large amounts of dislocations and defects, and driving recovery and recrystallization.

In this study, lower purity 3N silver was used to cast the discs used for HPT, and the effect of impurities and alloying additions in the Ag-1Ti and Ag-1Cu-1Pt alloys is considered responsible for the absence of significant recovery and loss of mechanical properties after storage at room temperature. It is believed that the use of lower purity silver and small amounts of alloying additions are effective at stabilizing the microstructure in UFG silver by impurities hindering of defect motion through the lattice [13], and by kinetic Zener pinning at grain

boundaries [5]. In literature, SPD processed 4N purity silver has been shown to undergo some self-annealing yet still retain an ultrafine grained microstructure after a year in storage, whereas 4N5 purity silver was found to fully recrystallize under the same conditions within 4 months [13]. It is therefore reasonable to conclude that although small, the increase in the impurity level from 4N to 3N is responsible for the retainment of a UFG microstructure and high hardness after storage for the 3N purity samples processed by HPT. The addition of alloying additions in the Ag-1 Ti and the Ag-1Cu-1Pt samples is responsible for the same effect as impurities on the stability of the alloys. Full microstructural analysis to validate the hypothesis of the pinning effect and correlations with the mechanical response will be the subject of a future publication.

3.4.2 Mechanical and Electrical Behavior

The stress-strain behavior of silver and silver alloys processed by HPT in this study was found to vary significantly based on both number of turns of HPT as well as by alloying additions, however several trends remain consistent across most measured samples. The reduced elongation in the material processed by HPT is consistent with other NC and UFG materials, which are known to undergo necking after very little plastic flow and work hardening [20,23]. As the grain size is extremely small in NC or UFG materials, plastic deformation facilitated by dislocation motion is reduced as dislocations emitted at grain boundaries are quickly annihilated at the opposite boundary of the ultrafine grains [22,23]. The unexpected increase in grain size with increasing amount of turns in the Ag-1Cu-1Pt material may be accounted for by recovery and recrystallization at the higher levels of strain that the 10-turn sample was subjected to during HPT processing. This is supported by the drop in average hardness seen in Ag-1Cu-1Pt in the 10-turn sample compared to the 6-turn sample after processing, as well as the gradual increase in SEM grain size measurements observed between the 4, 6, and 10-turn Ag-1Cu-1Pt material. This

indicates that there may be a saturation point of strain between 6 and 10 turns, past which the material begins to recover and dynamically recrystallize during HPT processing.

The UTS and yield strength of all material processed at 4 GPa* was found to correlate well with increased number of turns, consistent with the increased dislocation densities expected with more highly strained material. The higher pressure briefly applied to the 6-turn* 3N Ag disc during HPT processing is likely responsible for the nearly 40 MPa increase in the average UTS of the 6-turn* 3N Ag compared to all other samples tested, as higher applied pressure during processing is believed to suppress atomic diffusion and recovery during processing, yielding increased dislocation density and grain refinement [24]. This is supported by the large discrepancy of hardness values at equivalent strains for the 4-turn compared to the 6-turn* 3N Ag samples, as the equivalent strain does not account for increased pressure applied during HPT. There are clear differences in the work hardening potential of these alloys due to alloying and processing, however an in-depth understanding of these phenomena is reserved for a future study.

The HPT processing and alloying was found to have varying effects on the electrical conductivity of the processed material. Although most of the discrepancy in conductivity is believed to be dependent on the alloying additions used, both alloying and introduction of lattice defects are known to adversely affect the electrical conductivity of metals. Such disturbances in the lattice act as scattering sites for the electrons responsible for conductivity [14], and the reduced conductivity of the HPT material compared to the as-cast 3N silver is found to be consistent with the introduction of lattice defects such as grain boundaries and dislocations, as well as with the introduction of Ti, Cu and Pt alloying additions. The poorest conductivity was found in the material alloyed with 1% titanium by weight, which is consistent with other studies that have found that electrical conductivity is severely impacted by the addition of transition metal elements [14]. Electrical conductivity was found to increase with increasing strain in the

Ag-1Cu-1Pt samples, which is consistent with the increase in grain size and can be explained by possible dynamic recovery of the material at increased turns as mentioned previously. Conductivity in the 3N Ag HPT samples was found to have very little loss in conductivity compared to the as-cast condition due to the only sources of electron scattering coming from impurities and lattice defects introduced during processing.

In terms of balance between mechanical properties and electrical conductivity, Figure 6 may be considered. The datapoints from this study can be found distinctly divided into three groupings of points, dependent on alloying additions. Although the yield stress normalized by shear modulus for material from this study is not particularly notable, the normalized yield strength and conductivity of the HPT Ag-1Ti (the poorest performer in terms of conductivity) still rivals that of UFG aluminum. The HPT Ag-1Cu-1Pt, and in particular the HPT 3N Ag possess significantly higher conductivity at comparable normalized yield strength, with the 3N Ag surpassed only by annealed copper and silver. The strength presented for the HPT alloys in this study is also indicative only of these alloys with a UFG microstructure. With NC grains the hardness and yield strengths are found to be higher. This balance of good mechanical properties and excellent conductivity is promising for applications requiring higher mechanical strength than unprocessed silver while still retaining good electrical conductivity.

3.5 Conclusions

In this work, 3N purity silver and dilute silver alloys produced by casting were processed using high pressure torsion. The 3N purity silver and dilute silver alloys of Ag-1Ti and Ag-1Cu-1Pt were processed with this technique through a varying number of turns, and their response to processing followed by 36 months of room temperature storage was used to evaluate the microstructure, mechanical properties, electrical conductivity and thermal stability of these alloys. Processing by HPT was found to increase the Vickers microhardness from the as-cast

condition at all levels of strain for all the material tested. The highest increase in material processed at 4 GPa was 172%, 126%, and 149% in the 4-turn 3N Ag, 6-turn Ag-1Ti sample and 6-turn Ag-1Cu-1Pt samples, from their respective as-cast condition.

The thermal stability of silver and silver alloys processed by HPT was evaluated through Vickers microhardness measurements before and after 36 months in ambient temperature storage. All the alloys tested were found to retain a majority of the increased hardness induced by HPT processing as none of the material was found to fall to its pre-HPT processing level of hardness, indicating good long-term stability. The largest average losses in mechanical properties after storage for each alloy were 9 MPa, 4 MPa and 49 MPa, observed in the 6-turn 3N Ag*, 6-turn Ag-1Ti, and 4-turn Ag-1Cu-1Pt material respectively. It is believed that the use of lower purity silver and small amounts of alloying additions in the casting of the material used for HPT is responsible for the increase in thermal stability of this material compared to previous studies on the long-term thermal stability of silver [3,7,13] due to Zener pinning at grain boundaries and hindering of defect motion through the lattice.

Small-scale tensile samples cut from HPT processed discs were found to have increased yield strength and ultimate tensile strength, and reduced elongation compared to the as-cast condition. The best balance of electrical conductivity and mechanical properties was seen in the 3N Ag* processed by 6 turns* of HPT, which retained average IACS conductivity values of 97.5% with 0.2% average yield strength of 141 MPa and elongation to failure of 36% $\pm$ 4%. The addition of alloying elements was also found to significantly reduce the electrical conductivity due to higher incidence of electron scattering at lattice defects and alloying additions.

Increased pressure was found to have a large effect on the mechanical properties, as indicated by the 6-turn 3N Ag, which displayed the best Vickers microhardness and UTS of any of the material tested. Use of higher pressure during processing is believed to suppress atomic

diffusion and recovery during processing, yielding increased dislocation density and further refinement of grains compared to lower pressures.

Overall, processing of silver and silver alloys by HPT is found to be an effective method of producing bulk high strength silver alloys with good electrical conductivity and mechanical properties. The thermal stability of these alloys is found to be substantial after three years ambient storage at all levels of strain tested and is promising for high strength and high conductivity applications.

Acknowledgements

Erik Sease was supported in part by the Department of Education's Graduate Assistance in Areas of National Need (GAANN) fellowship. This research was supported by subcontract from QuesTek Innovations, LLC

Electron microscopy and microanalysis was performed on a ThermoFisher Scientific NNS450 in CFAMM at UC Riverside.

Conflicts of Interest: The authors declare no conflict of interest.

3.6 References

[1] Cordero, Z. C. et al, *Six decades of the Hall–Petch effect – a survey of grain-size strengthening studies on pure metals.* International Materials Reviews, 61(8), 495–512, (2016). doi:10.1080/09506608.2016.1191808

[2] E. O. Hall, *The Deformation and Ageing of Mild Steel: III Discussion of Results,* (1951), Proc. Phys. Soc. B 64 747

[3] J. Gubicza et al, *Principles of self-annealing in silver processed by equal-channel angular pressing: The significance of a very low stacking fault energy,* (2010), Materials Science and Engineering A 527 (2010) 752–760

[4] Schuh, C.A., Lu, K. *Stability of nanocrystalline metals: The role of grain-boundary chemistry and structure*. MRS Bulletin 46, 225–235 (2021). https://doi.org/10.1557/s43577-021-00055-x

[5] Atwater, M. A. et al. (2012). *The thermal stability of nanocrystalline copper cryogenically milled with tungsten*. Materials Science and Engineering: A, 558, 226–233. doi:10.1016/j.msea.2012.07.117

[6] Suryanarayana, C. (2002). *The structure and properties of nanocrystalline materials: Issues and concerns*. JOM, 54(9), 24–27. doi:10.1007/bf02709088

[7] J.P. Hirth, J. Lothe, *Theory of Dislocations*, Wiley, New York, 1982

[8] Valiev, R.Z. et al. *Producing bulk ultrafine-grained materials by severe plastic deformation*. JOM 58, 33–39 (2006). https://doi.org/10.1007/s11837-006-0213-7

[9] Hall EO (1951) The deformation and ageing of mild steel. 3: discussion of results. Proc Phys Soc Lond B 64:747–753

[10] Matsunaga, H., & Horita, Z. (2009). *Softening and Microstructural Coarsening without Twin Formation in FCC Metals with Low Stacking Fault Energy after Processing by High-Pressure Torsion*. Materials Transactions, 50(7), 1633–1637. doi:10.2320/matertrans.mf200921

[11] Gubicza, J., et al (2008). *Microstructure and yield strength of severely deformed silver*. Scripta Materialia, 58(9), 775–778. doi:10.1016/j.scriptamat.2007.12

[12] *Low Level Measurements Handbook Precision DC Current, Voltage, and Resistance Measurements*, 7th Edition. Keithley, A Tektronix Company, Copyright Tektronix.

[13] Hegedűs, Z. et al, (2011). *The effect of impurity level on ultrafine-grained microstructures and their stability in low stacking fault energy silver*. Materials Science and Engineering: A, 528(29-30), 8694–8699. doi:10.1016/j.msea.2011.08.034

[14] Cui, X. et al, (2017). *Study on the improvement of electrical conductivity and mechanical properties of low alloying electrical aluminum alloys*. Composites Part B: Engineering, 110, 381–387. doi.org/10.1016/j.compositesb.2016.11.042

[15] Metals Handbook, Vol.2 - Properties and Selection: Nonferrous Alloys and Special-Purpose Materials, ASM International 10th Ed. 1990.

[16] Zhilyaev, A., & Langdon, T. (2008). *Using high-pressure torsion for metal processing: Fundamentals and applications. Progress in Materials Science, 53(6), 893–979.* doi:10.1016/j.pmatsci.2008.03.002

[17] Holzwarth, U., & Gibson, N. *The Scherrer equation versus the 'Debye-Scherrer equation'*. Nature Nanotech 6, 534 (2011). https://doi.org/10.1038/nnano.2011.145

[18] Hegedűs, Z. et al, (2013). *Stability of the ultrafine-grained microstructure in silver processed by ECAP and HPT*. Journal of Materials Science, 48(13), 4637–4645. doi:10.1007/s10853-012-7124-5

[19] *Copper Wire Tables*, (Technical report). Circular of the Bureau of Standards No.31 (3d ed.). United States Department of Commerce. October 1, 1914. Available online: https://archive.org/details/copperwiretables31unituoft/page/n7/mode/2up

[20] Koch, C. (2003). *Optimization of strength and ductility in nanocrystalline and ultrafine grained metals*. Scripta Materialia, 49(7), 657–662. doi:10.1016/s1359-6462(03)00394-4

[21] Ke, X. et al, (2019). *Ideal maximum strengths and defect-induced softening in nanocrystalline-nanotwinned metals*. Nature Materials. doi:10.1038/s41563-019-0484-3

[22] Kurmanaeva, L., et al (2010). *Grain refinement and mechanical properties in ultrafine grained Pd and Pd–Ag alloys produced by HPT*. Materials Science and Engineering: A, 527(7-8), 1776–1783. doi:10.1016/j.msea.2009.11.001

[23] Hahn, E. N., and Meyers, M. A. (2015). *Grain-size dependent mechanical behavior of nanocrystalline metals*. Materials Science and Engineering: A, 646, 101–134. doi:10.1016/j.msea.2015.07.075

[24] Edalati, K., & Horita, Z. (2010). *Universal Plot for Hardness Variation in Pure Metals Processed by High-Pressure Torsion*. Materials Transactions, 51(5), 1051–1054. doi:10.2320/matertrans.m2009431

CHAPTER 4: CONCLUSIONS AND FUTURE RECOMMENDATIONS

This dissertation explores the processing-structure-properties-performance of bulk NC and UFG silver and silver alloys processed through top-down and bottom-up SPD methods.

In Chapter 2 the bottom-up synthesis of a high strength dilute silver alloy is investigated through mechanical alloying and spark plasma sintering, providing insights into the strengthening mechanisms in responsible for enhanced mechanical properties. Hall-Petch strengthening is determined to be responsible for roughly half of the strengthening of the synthesized material as compared to the annealed state of pure silver, with grain sizes reduced into the NC regime through processing. Solid solution strengthening from the addition of 1% titanium by weight, and Orowan strengthening from tungsten carbide contamination particles generated by mechanical alloying are believed to be the origin of the remaining sources of mechanical strength. Calculation of the Hall-Petch coefficients of silver synthesized through the methods used here imply higher hardness at equivalent grain sizes compared to pure silver, based off of coefficients of pure silver predicted by other studies in literature. Future recommendations for the bottom-up synthesis methods explored in Chapter 2 of this work include further exploration of Hall-Petch strengthening and Orowan strengthening with tungsten carbide dispersoids. The processing-structure-properties-performance relationship of these strengthening mechanisms is elucidated in this work, however the limitations of each are not. Further reduced grain sizes in milled Ag-1Ti powder are possible, as seen in the milled and unsintered powder. Coarsening due to the SPS process can be regulated with careful parameter control, therefore exploration of a lower grain size limit refinement before the onset of the reverse Hall-Petch effect is desirable, in order to determine an upper limit to strengthening through grain boundary refinement. Optimization of the Orowan strengthening mechanism is also desirable to determine a critical inter-particle distance and critical particle size to maximize Orowan strengthening as a balance of particle cutting versus

dislocation bowing around the particles in the microstructure. Further exploration of this material should include mechanical and electrical conductivity testing as seen in Chapter 3 of this dissertation.

In Chapter 3 the top-down synthesis of high strength 3N silver and two dilute silver alloys is investigated through high pressure torsion. The effects of plastic strain gradients and the addition of small amounts of impurities and dilute alloying additions are explored. Microstructural characterization prior and after long term storage at ambient temperature is analyzed to determine the effects of alloying and severe plastic deformation on the long-term microstructural stability and resistance to grain growth of these alloys. Silver of 99.9% purity, as well as silver alloys of Ag-1Ti and Ag-1Cu-1Pt are explored in this study to demonstrate the effectiveness of impurities versus alloying additions as grain pinning points. Small scale dogbone samples are cut from the processed material for mechanical testing and electrical conductivity measurements. These tests demonstrate excellent electrical conductivity rivaling that of pure silver and copper, with increased hardness, yield strength, and ultimate tensile strength. The reduced grain size in the processed material was found to reduce the elongation behavior of the material through the reduced ability of UFG scale grains to accommodate work hardening.

High strength UFG silver synthesized by high pressure torsion in Chapter 3 of this work is compared to the Hall-Petch plot generated from Ag-1Ti in Chapter 2 of this work and is found to lie within the expected range of hardness for the observed grain size, with an R^2 value of 0.94. This verifies that the hardness observed from HPT processing is due to grain refinement from HPT, rather than by other strengthening mechanisms. Future recommendations for the top-down synthesis methods explored in Chapter 3 of this work include further microstructural analysis of the processed material. The kinetic grain pinning effect of impurities and alloying additions and their effect on the mechanical properties observed during tensile testing is to be fully explored

and validated. The loss of mechanical properties observed in the most highly strained Ag-1Cu-1Pt sample, hypothesized to be due to dynamic recrystallization during processing is also to be fully explored and validated. Lastly, higher processing pressures should be further explored. As observed in the 6-turn 3N Ag, higher applied pressure is believed to introduce higher dislocation density as it suppresses atomic diffusion and recovery in the metal lattice, increasing hardness through Hall-Petch strengthening.

Overall, the work detailed in this dissertation promises bulk high strength silver alloys with excellent electrical conductivity, with resistance to self-annealing and grain growth at ambient temperature.